

# XXZ spin-1/2 representation of a finite- $U$ Bose-Hubbard chain at half-integer filling

Domenico Giuliano,<sup>1</sup> Davide Rossini,<sup>2</sup> Pasquale Sodano,<sup>3</sup> and Andrea Trombettoni<sup>4</sup>

<sup>1</sup>*Dipartimento di Fisica, Università della Calabria, Arcavacata di Rende I-87036, Cosenza, Italy & INFN, Gruppo collegato di Cosenza, Arcavacata di Rende I-87036, Cosenza, Italy*

<sup>2</sup>*NEST, Scuola Normale Superiore & Istituto Nanoscienze-CNR, I-56126 Pisa, Italy*

<sup>3</sup>*International Institute of Physics, Universidade Federal do Rio Grande do Norte, 59012-970, Natal, Brazil & INFN, Sezione di Perugia, Via A. Pascoli, I-06123, Perugia, Italy*

<sup>4</sup>*CNR-IOM DEMOCRITOS Simulation Center and SISSA, Via Bonomea 265 I-34136 Trieste, Italy & INFN, Sezione di Trieste, I-34127 Trieste, Italy*

Using a similarity Hamiltonian renormalization procedure, we determine an effective spin-1/2 representation of the Bose-Hubbard model at half-integer filling and at a finite on-site interaction energy  $U$ . By means of bosonization, we are able to recast the effective Hamiltonian as that of a spin-1/2 XXZ magnetic chain with pertinently renormalized coupling and anisotropy parameters. We use this mapping to provide analytical estimates of the correlation functions of the Bose-Hubbard model. We then compare such results with those based on DMRG numerical simulations of the Bose-Hubbard model for various values of  $U$  and for a number  $L$  of lattice sites as low as  $L \sim 30$ . We find an excellent agreement up to 10% between the output of analytical and numerical computations, even for relatively small values of  $U$ . Our analysis implies that, also at finite  $U$ , the 1D Bose-Hubbard model with suitably chosen parameters may be seen as a quantum simulator of the XXZ chain.

PACS numbers: 75.10.Pq, 75.10.Jm, 67.85.-d

## I. INTRODUCTION

The study of magnetic systems is one of the most active fields of research in condensed matter physics<sup>1</sup>: the variety of emerging ground-states, as well as the rich phase diagram of magnetic lattices, makes these systems an optimal testbed to probe the competition between various orders and frustration effects<sup>2</sup>. From this perspective, it would be very useful to be able to engineer synthetic physical systems effectively describing magnetic model Hamiltonians, with tunable geometry and parameters.

A promising route is provided by cold atomic setups: for instance, itinerant magnetism in bulk ultracold Fermi systems with repulsive interactions has been experimentally studied<sup>3</sup>, while small spin networks have been simulated with ion chains<sup>4</sup>. Effective nearest-neighbour spin-spin interactions for atoms in neighbour wells of an optical lattice may result from super-exchange couplings: the corresponding second-order tunneling has been observed in array of double wells<sup>5</sup>. Furthermore, using fast oscillations of the optical lattice, it is possible to control the sign of the nearest-neighbour tunneling<sup>6</sup>, which has been recently used to simulate classical frustrated magnetism in triangular lattices<sup>7</sup>. One may also use two-component gases where the two internal degrees of freedom correspond to the simulated (pseudo)spins. Spin interactions can be tuned by adjusting the external potential<sup>8</sup>. The recent realization of controllable Bose-Bose mixtures<sup>9</sup> paves the way towards the experimental simulation of spin Hamiltonians, in which the atomic counterpart of magnetic phases, like antiferromagnetic Néel and XY ferromagnetic phases (respectively corresponding to the checkerboard and the supercounterfluid phases<sup>10</sup>) may be detected and studied.

A key tool in the manipulation of ultracold atomic sys-

tems is the possibility to superimpose and control optical lattices<sup>11</sup>. The low-energy properties of ultracold bosons in deep optical lattices are well captured by the Bose-Hubbard (BH) Hamiltonian:<sup>12</sup>

$$H_{\text{BH}} = \sum_{\langle i,j \rangle} \left[ -t(b_i^\dagger b_j + b_j^\dagger b_i) + V n_i n_j \right] + \frac{U}{2} \sum_i n_i (n_i - 1). \quad (1)$$

In Eq. (1),  $\langle i, j \rangle$  stands for any pair of nearest neighbouring sites, while the operators  $b_i^\dagger$  ( $b_i$ ), with  $[b_i, b_j^\dagger] = \delta_{i,j}$  and  $n_i = b_i^\dagger b_i$ , create (annihilate) a boson in the site  $i$ . The parameter  $t$  denotes the hopping strength, and  $U$  ( $V$ ) is the interaction energy of two particles at the same site (at two nearest neighbouring sites).

The use of optical lattices in ultracold atomic systems is also central in other proposals to simulate spin Hamiltonians, such as the quadratic-biquadratic spin model<sup>13</sup>, or antiferromagnetic spin chains<sup>14</sup>. Following the latter suggestion, by means of a tilted 1D optical lattice, the Ising chain in a transverse field was experimentally simulated<sup>15</sup>. The paramagnetic, as well as the antiferromagnetic phase (and the corresponding quantum phase transition), were detected by measuring the probability to have an odd occupation of sites, while the formation of magnetic domains was observed using in-situ site-resolved imaging and noise correlation measurements<sup>15</sup>.

For very large values of  $U$ , i.e. for  $t/U \ll 1$ , the BH model can be mapped into the Heisenberg XXZ spin-1/2 Hamiltonian:

$$H_{\text{XXZ}} = -J \sum_{\langle i,j \rangle} (s_i^x s_j^x + s_i^y s_j^y - \Delta s_i^z s_j^z), \quad (2)$$

where  $\vec{s}_i = \vec{\sigma}_i/2 = (s_i^x, s_i^y, s_i^z)$  are the  $S = 1/2$  spin operators,  $\vec{\sigma}_i$  being the Pauli matrices,  $J$  is the nearest-neighbour coupling, and  $\Delta$  is the anisotropy parameter

( $\Delta = \pm 1$  respectively correspond to the antiferromagnetic and the ferromagnetic isotropic Heisenberg model).

The use of lattice spin systems for interacting bosons traces back to the classical papers by Matsubara and Matsuda in the 50's, where the properties of helium II were studied assuming that each atom can occupy one of the lattice points<sup>16</sup>. The further assumption that two atoms cannot simultaneously occupy the same lattice site (due to the hard-core part of the interparticle interaction between Helium atoms<sup>17</sup>) leads to an effective spin model in a magnetic field<sup>16</sup>. To qualitatively understand the emergence of a spin representation of the one-component BH model one may say that, for  $U \rightarrow \infty$  and *if* two states per site give a dominant contribution to the energy, an XXZ Hamiltonian is retrieved: this is exactly what happens when the filling  $f$ , defined as the average number of bosons per lattice site, is half-integer. Indeed, for  $f = \bar{n} + 1/2$ , with  $\bar{n}$  integer, the relevant states in the Fock space are given by  $|\bar{n}\rangle$  and  $|\bar{n} + 1\rangle$  (deviations from half-integer fillings would result in a magnetic term in the XXZ Hamiltonian). For half-integer  $f$ , at the leading order in  $t/U \rightarrow 0$  one has  $J = 2t(f + 1/2)$  and  $\Delta = V/J$  (see the discussion in Sec. III).

The XXZ model is a paradigmatic spin Hamiltonian which has been the object of many investigations and that in 1D is exactly solvable by Bethe ansatz<sup>18,19</sup>; this provides an ideal arena to test different analytical and numerical techniques, from bosonization<sup>20,21</sup> to density matrix renormalization group (DMRG)<sup>22</sup>. The study of (static and dynamical) correlation functions in this model is currently an active area of research<sup>23-32</sup> and exact analytical results for the correlation functions at small distance (both at zero and finite temperature) are by now available<sup>25</sup>. The asymptotic form of the ground-state correlation functions in the thermodynamic limit is power-law with an exponent that has been obtained by comparing the result of abelian bosonization with the Bethe ansatz solution<sup>33</sup>: for an open chain in the region  $-1 \leq \Delta \leq 1$ , the numerical findings for correlation functions obtained with DMRG were compared with the results of a low-energy field theory, showing a very good agreement and allowing for precise estimates of the amplitudes of the correlation functions<sup>34</sup>. In turn, the obtained amplitudes were found in agreement with the analytical expressions given by Lukyanov and Zamolodchikov<sup>35,36</sup>. Finally, exact results for the XXZ chain in a special scaling limit were used to compute the local correlations of a continuous Lieb-Liniger 1D Bose-gas<sup>37</sup>.

In this paper we determine a correspondence between the BH chain at half-integer filling for *finite*  $U$  and a 1D XXZ spin-1/2 model. This enables us to provide analytical expressions for the BH correlation functions, which we compare with numerical results obtained with DMRG, showing that there is a very good agreement both at large and small distances and also for  $U/J$  as low as  $\sim 2$  and for a number of sites  $L \geq 30$ . As a consequence, the numerical determination of the superfluid to charge-density-wave and superfluid to Mott-insulator phase transitions

(respectively corresponding, in the effective XXZ chain, to  $\Delta_{\text{eff}} = 1$  and  $\Delta_{\text{eff}} = -1$ ) well agrees with the analytical results for the XXZ chain. Using our approach, we are able not only to provide analytical expressions for the 1D BH correlation functions, but also to show that the BH chain at half-integer filling provides a reliable quantum simulator of the XXZ chain.

In the following we derive an effective spin-1/2 Hamiltonian for the BH chain at half-integer filling as a power series of  $t/U$ . Following Refs. 38,39, we perform a continuous unitary transformation  $\mathbf{S}$  which block-diagonalizes the Hamiltonian in the basis of the eigenvectors of  $H_{\text{BH}}$  with  $t = 0$  and determine  $\mathbf{S}$  perturbatively to the order  $(t/U)^2$  (a similar technique has been used in Ref. 40 for the fermionic Hubbard model). We finally show that, using bosonization, this Hamiltonian can be recast in the XXZ form with pertinent coupling and anisotropy parameters. We observe that, while to the first order in  $t/U$  one finds a XXZ model with  $J = 2t(f + 1/2)$  and  $\Delta = V/J$ , to the next order in  $t/U$  one gets an effective spin Hamiltonian which is not of the XXZ form, since it also contains next-nearest neighbours and 3-spin terms (this is the bosonic counterpart of a similar computation done for the 1D, as well as for the 2D, Fermi-Hubbard model<sup>41-43</sup>, where 4-spin terms appear). However, in 1D it is possible to proceed further using bosonization: introducing a Luttinger liquid description of the effective Hamiltonian, we are able to incorporate the long-wavelength behaviour of non-XXZ terms in the effective coupling and anisotropy parameters,  $J_{\text{eff}}$  and  $\Delta_{\text{eff}}$ , which are now function of  $t$ ,  $V$ ,  $f$  and  $U$ .

The plan of the paper is the following: after introducing the BH and the XXZ models and recalling some useful properties and results (Sec. II), we employ the continuous unitary transformation introduced by Glazek and Wilson<sup>38</sup> to approximate the BH chain at half-integer filling with an effective spin-1/2 Hamiltonian (Sec. III). In Sec. IV we use bosonization to recast this effective Hamiltonian as an XXZ Hamiltonian, with coupling  $J_{\text{eff}}$  and anisotropy  $\Delta_{\text{eff}}$ , while in Sec. V we establish the correspondence between the correlation functions of the BH model and the ones of the XXZ chain. We then proceed in comparing the analytical results obtained for the BH correlation functions with the numerical findings obtained by DMRG numerical simulations (Sec. VI), both for the correlation functions and the phase transition points. Section VII is devoted to our conclusions, while more technical details are contained in the Appendices.

## II. MODEL HAMILTONIANS

Let us start by reviewing the basic properties of the BH and of the spin-1/2 XXZ Hamiltonians, in particular focusing on known analytical results about the real-space spin correlations in the XXZ chain.

### A. Bose-Hubbard model

The low-energy properties of interacting bosons in a one-dimensional deep optical lattice are in general well described by the Bose-Hubbard Hamiltonian (1), which, in 1D and with open boundaries, reads:

$$H_{\text{BH}} = -t \sum_{i=1}^{L-1} \left( b_i^\dagger b_{i+1} + b_{i+1}^\dagger b_i \right) + \frac{U}{2} \sum_{i=1}^L n_i (n_i - 1) + V \sum_{i=1}^{L-1} n_i n_{i+1}. \quad (3)$$

We denote with  $N$  the total number of particles in the  $L$ -site chain, so that the filling  $f$ , that is, the average number of particles per site, is given by  $f = \frac{N}{L}$ . For alkali atoms usually  $V \ll U$ , but with dipolar gases (or polar molecules)  $V$  could be comparable with  $U$ : experiments with dipolar gases<sup>44</sup> and long-lived ground-state polar molecules<sup>45</sup> in optical lattices have been already performed (see also the review in Ref. 46).

A large amount of experiments investigated the properties of the BH model: the main reason for this interest lies on the fact that this model exhibits a quantum phase transition between a superfluid phase (for  $t/U \gg 1$ ) and a Mott insulator (for  $t/U \ll 1$ )<sup>47</sup>. A finite  $V$  generally favours charge-density-wave phases: e.g., for half-integer filling  $f = 1/2$ , a large  $V \gg t, U$  will result in a ground-state of the type  $|1, 0, 1, 0, \dots\rangle$  (where in general  $|n_1, n_2, n_3, \dots\rangle$  is an eigenfunction of  $H_{\text{BH}}$  with  $t = 0$ ). The ground-state of the BH model has been studied in the seminal paper in Ref. 47 using the grand-canonical ensemble, where the chemical potential  $\mu$  is introduced to enforce the constraint on the number of particles. The phase diagram in the  $U - \mu$  plane shows the characteristic lobes: for a pertinently fixed value of  $\mu$ , the half-integer fillings correspond to the ‘‘basis’’ of the lobes (i.e. where the lobes touch) and, for  $V = 0$ , one has a superfluid for each finite value of  $t$ , while a finite and positive value of  $V$  gives rise to a charge-density-wave region among the Mott lobes.

The Mott-insulator/superfluid transition was first observed in 3D<sup>48</sup> and subsequently in 1D<sup>49</sup> and 2D<sup>50</sup>. The effect of a superimposed external potential (typically a parabolic one) has been also considered: the so-called wedding-cake-like density has been studied both theoretically<sup>51,52</sup> and experimentally<sup>53,54</sup>. The coherence properties of ultracold bosons in optical lattices have been studied, as well, showing that phase coherence on short length scales still persists deep in the insulating phase<sup>55</sup>. The BH model in a 1D geometry can be obtained either by tightly confining the bosonic cloud in two radial directions in presence of a periodic potential in the transverse direction, or by creating many (eventually uncoupled) tubes with a 2D optical lattice. The properties of strongly correlated phases across the superfluid to Mott-insulator phase transition have been analyzed in 1D by means of Bragg spectroscopy<sup>56</sup>. The excitation spectrum

in the strongly interacting regime has been also studied in presence of a tunable disorder, created by a bichromatic optical lattice, showing a broadening of the Mott-insulator resonances<sup>57</sup>.

The finite- $V$  1D BH model has been studied with a number of analytical and numerical techniques: in particular in Ref. 58 the phase boundaries of the Mott insulators and charge-density-wave phases were determined by DMRG. The zero-temperature phase diagram both of the BH model and of a spin- $S$  Heisenberg model was constructed and their relation investigated<sup>59</sup>. The role of  $V$  in inducing supersolid phases in the BH chain was also studied<sup>60-63</sup>. Bosonization techniques have been applied as well to BH chains, providing a very effective way to compute the correlation functions and their decay at large distance<sup>64</sup>.

Finally, we mention that the effect of intersite interactions was considered since the 90’s in the related quantum phase model, describing Josephson junction arrays<sup>65</sup>: this can be obtained from the BH model for large filling per site when the number fluctuations are negligible in the kinetic term. The chemical potential term in the BH model corresponds to the so-called ‘‘offset charge’’  $q$ , which are external charges present in the superconducting network<sup>65</sup>: the lobes in the quantum phase model are equal, since there is an invariance for  $q \rightarrow q + 2e$  ( $2e$  being the charge of the Cooper pairs), and an half-integer value of the filling  $f$  corresponds to half-integer values of the offset charges  $q/2e$ . The study of intersite interactions is relevant in Josephson junction arrays since the interaction term depends on the capacitance matrix  $C_{ij}$ , which is in general not diagonal, resulting in terms of the form  $V_{ij} n_i n_j$ , where  $V_{ij} \propto (C_{ij})^{-1}$ : as a mean-field analysis shows<sup>66</sup>, for a diagonal capacitance matrix one has that at  $T = 0$  the superconducting phase is obtained for each value of the Josephson energy  $E_J$  ( $\propto t$  in the mapping) and that at  $q = e$  one has a finite critical temperature for the Mott-insulator/superfluid transition for each finite value of  $E_J$  (unlike  $q = 0$ , where a critical value of  $E_J$  is required). Non-diagonal terms of the capacitance matrix favour charge density waves<sup>65</sup>: the role of the intersite terms was considered for superconducting chains and the corresponding phase diagram investigated<sup>67,68</sup>, revealing that in 1D a (superconducting) repulsive Luttinger liquid phase exists. The opening of Luttinger liquid phases with tunable parameters also allows for designing Josephson junction networks supporting emerging two-level quantum systems with a high level of quantum coherence<sup>69-71</sup>.

To conclude this section let us mention that, in the rest of the paper, we will mostly deal with half-integer fillings,  $f \equiv \bar{n} + \frac{1}{2}$ , with  $\bar{n} = 0, 1, 2, \dots$ . The reason for such a choice is that in this case the relevant states for the description of system for  $U \rightarrow \infty$  are just  $|\bar{n}\rangle$  and  $|\bar{n} + 1\rangle$ . Simple arguments, reviewed in Sec. II B, then show that, to first order in  $t/U$ , the BH Hamiltonian is mapped into an XXZ spin-1/2 Hamiltonian which is integrable in 1D. Within the XXZ-model framework, it is also possible to consider small deviations from the half-

filled regime, which mainly give rise to a uniform magnetic field in the  $z$ -direction. Even though we will not consider large fluctuations in  $f$  (of order 1), it is possible to take them into account, by keeping, as relevant states for  $U \rightarrow \infty$ ,  $|\bar{n}\rangle$ ,  $|\bar{n}-1\rangle$ ,  $|\bar{n}+1\rangle$ . In this case, an effective spin-1 XXZ effective model (in general not integrable) is expected<sup>72</sup>. Spin-1 models exhibit a gapped (Haldane) insulator phase<sup>73,74</sup>, which has been investigated in the context of the 1D BH model<sup>75–78</sup>.

## B. XXZ chain

For a chain with  $L$  sites and open boundaries, the Hamiltonian of a spin-1/2 XXZ model given in Eq. (2) particularizes to:

$$H_{\text{XXZ}} = -J \sum_{i=1}^{L-1} (s_i^x s_{i+1}^x + s_i^y s_{i+1}^y - \Delta s_i^z s_{i+1}^z). \quad (4)$$

The global minus sign in the couplings has been introduced in order to more easily perform the comparison with the BH model, and it can be readily gauged away by implementing the canonical mapping to the spin-1/2 operators  $\tau_j^a$  defined as  $\tau_j^{x,y} = (-1)^j s_j^{x,y}$ ,  $\tau_j^z = s_j^z$ . Therefore the chain is antiferromagnetic (ferromagnetic) for  $\Delta$  positive (negative).

Following Ref. 16, one can derive the Hamiltonian in Eq. (4) from the BH Hamiltonian (3) at half-integer filling  $f$  and for  $U \rightarrow \infty$ . To do so, let us define  $s_j^z \equiv n_j - f$  (so that the eigenvalues of  $s_j^z$  are  $\pm \frac{1}{2}$ ). Since for  $t = 0$  the energy per particle is (for  $L \rightarrow \infty$ )  $\varepsilon = Uf(f-1)/2 + Vf^2$ , it follows that  $H_{\text{BH}} \xrightarrow{t \rightarrow 0} V s_j^z s_{j+1}^z$ , i.e.

$$J\Delta \equiv V. \quad (5)$$

Similarly, for  $f \gg 1$ , one gets  $J \approx 2tf$  as one can see by putting  $b_i \sim \sqrt{f} e^{i\phi_i}$  and mapping the obtained result in the XXZ spin-1/2 language<sup>67</sup>: for finite values of  $f$  one gets (see Sec. III)

$$J \equiv 2t \left( f + \frac{1}{2} \right). \quad (6)$$

Eqs. (5, 6) provide the desired mapping between the BH model and the XXZ Hamiltonian to lowest order in  $t/U$ . However, as we are going to see in Sec. V, to get a quantitative agreement between the BH and the XXZ correlation functions even for  $t/U$  relatively small (as low as 0.1 for  $f = 1/2$ ) one has to go to the next order in  $t/U$ : the corresponding Hamiltonian is determined in Sec. III and recast in XXZ form via a Luttinger representation in Sec. IV. We remark that, since our result are obtained at half-integer filling, we may omit the addition of a magnetic field term of the form  $\propto \sum_{i=1}^L s_i^z$  to Eq. (4). Indeed such a term is proportional to the total spin  $S_T^z = \sum_{i=1}^L s_i^z$  in the  $z$  direction and, since the system is half-filled, only eigenstates of  $H_{\text{XXZ}}$  with  $S_T^z = 0$

are physically meaningful - notice that in the following analytical results based on the XXZ Hamiltonian (4) are compared with numerical DMRG simulations of the BH chain in the canonical ensemble, where  $\sum_i n_i$  is conserved and equal to  $N$ .

The Hamiltonian  $H_{\text{XXZ}}$  is exactly solvable by means of standard Bethe ansatz techniques<sup>18,19</sup>: however, explicitly computing the real-space spin-spin correlation functions is quite a difficult task. Exact analytical results for short-range correlators in a range of up to seven lattice sites were reported for the isotropic Heisenberg model in Ref. 31, in the thermodynamic limit ( $L \rightarrow \infty$ ) and at arbitrary finite temperature, and for finite chains of arbitrary length  $L$  in the ground-state. Results for short-range correlation functions are also available for the XXZ chain<sup>25</sup>. For large distances, using the standard bosonization approach<sup>20,21</sup> to spin-1/2 XXZ model<sup>79</sup>, one may find out all the spin-spin correlation functions in terms of two-point correlators of pertinent conformal operators<sup>34</sup>: in the thermodynamic limit one finds the asymptotic forms

$$\langle \psi_0 | s_i^z s_j^z | \psi_0 \rangle = (-1)^{i-j} \frac{A_z}{|i-j|^{1/\eta}} - \frac{1}{4\pi^2 \eta (i-j)^2}, \quad (7)$$

$$\langle \psi_0 | s_i^x s_j^x | \psi_0 \rangle = (-1)^{i-j} \frac{A_x}{|i-j|^\eta} - \frac{\tilde{A}_x}{|i-j|^{\eta+1/\eta}}, \quad (8)$$

where  $|\psi_0\rangle$  is the ground-state of  $H_{\text{XXZ}}$  and we set<sup>33</sup>

$$\eta = 1 - \frac{1}{\pi} \arccos \Delta. \quad (9)$$

Analytical expressions for the correlation amplitudes  $A_x$ ,  $\tilde{A}_x$  and  $A_z$  entering Eqs. (7, 8) were presented in Refs. 35, 36 and further discussed in Ref. 80 (see also the discussion in Sec. V of Ref. 32):

$$A_x = \frac{\mathcal{A}^\eta}{8(1-\eta)^2} e^{-\mathcal{I}_x}, \quad (10)$$

$$\tilde{A}_x = \frac{\mathcal{A}^{\eta+1/\eta}}{2\eta(1-\eta)} e^{-\tilde{\mathcal{I}}_x}, \quad (11)$$

$$A_z = \frac{2\mathcal{A}^{1/\eta}}{\pi^2} e^{\mathcal{I}_z}, \quad (12)$$

with

$$\mathcal{I}_x = \int_0^\infty \frac{dt}{t} \left( \frac{\sinh(\eta t)}{\sinh(t) \cosh[(1-\eta)t]} - \eta e^{-2t} \right),$$

$$\tilde{\mathcal{I}}_x = \int_0^\infty \frac{dt}{t} \left( \frac{\cosh(2\eta t) e^{-2t} - 1}{2 \sinh(\eta t) \sinh(t) \cosh[(1-\eta)t]} + \frac{1}{\sinh(\eta t)} - \frac{\eta^2 + 1}{\eta} e^{-2t} \right),$$

$$\mathcal{I}_z = \int_0^\infty \frac{dt}{t} \left( \frac{\sinh[(2\eta-1)t]}{\sinh(\eta t) \cosh[(1-\eta)t]} - \frac{2\eta-1}{\eta} e^{-2t} \right),$$

and

$$\mathcal{A} = \frac{\Gamma\left(\frac{\eta}{2(1-\eta)}\right)}{2\sqrt{\pi}\Gamma\left(\frac{1}{2(1-\eta)}\right)}, \quad (13)$$

and  $\Gamma(x)$  being the Euler's Gamma function.

Analytical expressions (in the large- $L$  limit) for the subsequent prefactors of the correlation functions are reported in Refs. 27,32.

For chains of finite size  $L$  with open boundary conditions, one obtains<sup>34</sup>:

---


$$\begin{aligned} \langle \psi_0 | s_i^z s_j^z | \psi_0 \rangle &= \frac{(-1)^{i-j} a^2}{2f_{\frac{1}{2\eta}}(2i)f_{\frac{1}{2\eta}}(2j)} \left( \frac{f_{\frac{1}{\eta}}(i+j)}{f_{\frac{1}{\eta}}(i-j)} - \frac{f_{\frac{1}{\eta}}(i-j)}{f_{\frac{1}{\eta}}(i+j)} \right) - \frac{1}{4\pi^2\eta} \left( \frac{1}{f_2(i-j)} + \frac{1}{f_2(i+j)} \right) \\ &\quad - \frac{a}{2\pi\eta} \left\{ \frac{(-1)^i}{f_{\frac{1}{2\eta}}(2i)} [g(i-j) + g(i+j)] - \frac{(-1)^j}{f_{\frac{1}{2\eta}}(2j)} [g(i-j) - g(i+j)] \right\} \end{aligned} \quad (14)$$

and

$$\begin{aligned} \langle \psi_0 | s_i^x s_j^x | \psi_0 \rangle &= \frac{f_{\frac{\eta}{2}}(2i)f_{\frac{\eta}{2}}(2j)}{f_{\eta}(i-j)f_{\eta}(i+j)} \left\{ (-1)^{i-j} \frac{c^2}{2} - \frac{b^2}{4f_{\frac{1}{2\eta}}(2i)f_{\frac{1}{2\eta}}(2j)} \left[ \frac{f_{\frac{1}{\eta}}(i+j)}{f_{\frac{1}{\eta}}(i-j)} + \frac{f_{\frac{1}{\eta}}(i-j)}{f_{\frac{1}{\eta}}(i+j)} \right] \right. \\ &\quad \left. - \frac{bc}{2} \operatorname{sgn}(i-j) \left[ \frac{(-1)^i}{f_{\frac{1}{2\eta}}(2j)} - \frac{(-1)^j}{f_{\frac{1}{2\eta}}(2i)} \right] \right\}, \end{aligned} \quad (15)$$

where  $\operatorname{sgn}(x)$  is the sign function and

$$f_{\alpha}(x) = \left[ \frac{2(L+1)}{\pi} \sin\left(\frac{\pi|x|}{2(L+1)}\right) \right]^{\alpha}, \quad (16)$$

$$g(x) = \frac{\pi}{2(L+1)} \cot\left(\frac{\pi x}{2(L+1)}\right), \quad (17)$$

with

$$\frac{c^2}{2} \equiv A_x, \quad \frac{b^2}{4} \equiv \tilde{A}_x, \quad \frac{a^2}{2} \equiv A_z \quad (18)$$

(here and in the following all the distances are in units of the lattice constant).

The agreement between exact numerical calculations of the XXZ correlation functions and analytical expressions in (14, 15) is very good, and it becomes excellent with  $L \sim 100$  for  $-0.8 \lesssim \Delta \lesssim 0.8$ <sup>34</sup>. Thus one may readily assume that Eqs. (14, 15) provide quite an accurate analytical expression for the spin-spin correlation functions in the XXZ model<sup>81</sup>. As a consequence, constructing a rigorous mapping between the BH and the XXZ spin-1/2 Hamiltonian and expressing correlation functions of one model in terms of the ones of the other model gives an efficient and straightforward way to provide accurate analytic expressions for real-space correlation functions in the BH model at half-integer filling.

We finally observe that the only system-dependent parameter determining the spin-spin correlation functions is the coefficient  $\eta$ : thus, in tracing out the mapping between the two models, this is the key quantity to be calculated as a function of the BH parameters. In particular,

one may distinguish between the regions in parameter space with  $\eta > 1/2$  and  $\eta < 1/2$ : while the former one corresponds to an antiferromagnetic spin chain, the latter one (which may be realized for pertinently chosen values of the parameters of  $H_{\text{BH}}$ , as we shall show below) corresponds to a ferromagnetic chain.

### III. EFFECTIVE SPIN-1/2 HAMILTONIAN FOR THE BOSE-HUBBARD MODEL AT HALF-INTEGERS FILLING

As reviewed in the previous section, for  $U \rightarrow \infty$ , the BH Hamiltonian maps onto the XXZ model in Eq. (4), with the parameters  $J, \Delta$  given in Eqs. (5, 6). This may be seen as a first-order term in an expansion (in powers of  $t/U$ ) aimed at computing the effective Hamiltonian: in this section we compute this effective Hamiltonian to the next order. As we shall show in the following, this is enough to fit quite well the numerical data for the correlation functions of the BH model using the analytical results obtained for the correlators of the XXZ chain.

To approach the large- $U$  limit one may either proceed by performing a strong coupling expansion to the second or higher-order of perturbation theory, or by deriving effective Hamiltonians using alternative techniques, based on canonical transformations or continuous unitary transformations<sup>82</sup>. At integer filling, for instance, it is possible to evaluate the energy of the Mott insulator and of the superfluid state in higher-order perturbation theory and determine the phase diagram in the  $U - \mu$

plane<sup>83</sup>. Since we are rather interested to the BH at half-integer filling, i.e., in the region of the phase diagram where the lobes touch and the superfluid phase persists also at very small  $U$  (with  $V = 0$ ), we found it convenient to use an approach based on continuous unitary transformations<sup>38,39</sup>. We follow the notation and the method presented in the paper by Glazek and Wilson (GW)<sup>38</sup>: systematically using the GW renormalization procedure, we work out an effective description of the dynamics of the BH model, restricted to the low-energy subspace determined by the constraint on the total number of particles and by the large- $U$  assumption. As a result, the low-energy subspace is spanned by states with either  $\bar{n}$  or  $\bar{n} + 1$  particles per site, with the total number of particles being fixed to  $N$ . Thus, the space of physically relevant states at each site is in one-to-one correspondence with the Hilbert space of states of a quantum spin-1/2 degree of freedom; we shall see that, at half-integer filling, even for finite  $U$  the BH model may be replaced by an effective spin-1/2 Hamiltonian, with pertinently determined parameters. The method amounts to an iterative block-diagonalization of the BH Hamiltonian on the space of eigenfunctions of  $H_{\text{BH}}$  with  $t = 0$ .

To illustrate the procedure, we start from the explicit construction of the “low-energy” Hilbert space of physically relevant states, in the large- $U$  limit. Neglecting excitations with energy  $\sim U$  amounts to truncating the Hilbert space to a subspace  $\mathcal{F}$ , defined as

$$\mathcal{F} = \text{Span}\{|\bar{n} + \mu_1, \dots, \bar{n} + \mu_L\rangle\}, \quad (19)$$

with  $\mu_i$  taking the values  $\mu_i = 0, 1$  and  $\sum_{i=1}^L \mu_i = \frac{L}{2}$ . In Eq. (19)  $|n_1, \dots, n_L\rangle$  labels the state in the Hilbert space with  $n_i$  particles on site  $i$ . To implement the GW approach, one splits the Hamiltonian (3) as  $H_{\text{BH}} = H_0 + H_I$ , with

$$H_0 = \frac{U}{2} \sum_i n_i(n_i - 1) + V \sum_i n_i n_{i+1} \quad (20)$$

$$H_I = -t \sum_i (b_i^\dagger b_{i+1} + b_{i+1}^\dagger b_i). \quad (21)$$

From Eqs. (20, 21) one sees that  $H_0$  is diagonal with respect to the partition of the Hilbert space into  $\mathcal{F}$  plus its orthogonal complement, since

$$H_0|n_1, \dots, n_L\rangle = E_0[n_1, \dots, n_L]|n_1, \dots, n_L\rangle \quad (22)$$

with  $E_0[n_1, \dots, n_L] = (U/2) \sum_i n_i(n_i - 1) + V \sum_i n_i n_{i+1}$ , while  $H_I$  exhibits off-diagonal (with respect to the partition of the Hilbert space) matrix elements which are  $\mathcal{O}(t\bar{n})$ . In order to block-diagonalize  $H_{\text{BH}}$ , one needs to perform a *similarity* transformation<sup>38</sup>

$$H_{\text{BH}} \rightarrow \tilde{\mathcal{H}}_{\text{BH}} = \mathbf{S}^\dagger H_{\text{BH}} \mathbf{S}, \quad (23)$$

with  $\mathbf{S}$  unitary. Upon setting  $\mathbf{S} = \mathbf{I} + \mathbf{T}$ , the unitarity of  $\mathbf{S}$  implies the optical theorem

$$\mathbf{T} + \mathbf{T}^\dagger + \mathbf{T}^\dagger \mathbf{T} = 0. \quad (24)$$

Setting  $\mathbf{T} \equiv \mathbf{h} + \mathbf{a}$ , with

$$\mathbf{h} = \frac{1}{2} (\mathbf{T} + \mathbf{T}^\dagger), \quad \mathbf{a} = \frac{1}{2} (\mathbf{T} - \mathbf{T}^\dagger) \quad (25)$$

one finds that Eq. (24) yields

$$\mathbf{h} = \frac{1}{2} (\mathbf{a}^2 - \mathbf{h}^2). \quad (26)$$

Eq. (26) shows that  $\mathbf{h}$  is always “higher order” than  $\mathbf{a}$ . Following Ref. 38, it is most convenient to define the new interaction Hamiltonian  $\tilde{\mathcal{H}}_I$  as

$$\tilde{\mathcal{H}}_I = \tilde{\mathcal{H}}_{\text{BH}} - H_0 \quad (27)$$

so that the new “free” Hamiltonian is the same as the old one ( $H_0$ ).

To further proceed and determine  $\mathbf{S}$ , one has to require that the matrix elements of  $\tilde{\mathcal{H}}_I$  between states with energy difference  $\gtrsim U$  are equal to zero, amounting to state that  $\tilde{\mathcal{H}}_I$  is block-diagonal with respect to the partition of the Hilbert space into  $\mathcal{F}$  plus its orthogonal complement, i.e.

$$\mathcal{P} \tilde{\mathcal{H}}_I \mathcal{P} + (\mathbf{I} - \mathcal{P}) \tilde{\mathcal{H}}_I (\mathbf{I} - \mathcal{P}) = \tilde{\mathcal{H}}_I, \quad (28)$$

where  $\mathcal{P}$  is the projector onto  $\mathcal{F}$  and  $\mathbf{I} - \mathcal{P}$  the projector onto its complementary subspace<sup>84</sup>. One sees that Eq. (28) implies that

$$\mathcal{P} \tilde{\mathcal{H}}_I (\mathbf{I} - \mathcal{P}) = (\mathbf{I} - \mathcal{P}) \tilde{\mathcal{H}}_I \mathcal{P} = 0. \quad (29)$$

Using Eqs. (23, 25, 27), one may write  $\tilde{\mathcal{H}}_I$  as

$$\tilde{\mathcal{H}}_I = (\mathbf{I} + \mathbf{h} - \mathbf{a})(H_0 + H_I)(\mathbf{I} + \mathbf{h} + \mathbf{a}) - H_0 \quad (30)$$

and Eq. (29) then becomes

$$\mathcal{P}\{H_I + \{H_0, \mathbf{h}\} + [H_0, \mathbf{a}] + \mathbf{T}^\dagger H_I + H_I \mathbf{T} + \mathbf{T}^\dagger H_I \mathbf{T}\} (\mathbf{I} - \mathcal{P}) = 0. \quad (31)$$

Eq. (31), together with the identity

$$\mathbf{a} = \mathcal{P} \mathbf{a} (\mathbf{I} - \mathcal{P}) + (\mathbf{I} - \mathcal{P}) \mathbf{a} \mathcal{P} \quad (32)$$

and with Eq. (26), is all what one needs in principle to fully determine  $\mathbf{a}$  and  $\mathbf{h}$  (and, therefore, the operator  $\mathbf{T}$ ).

However, except for some simple cases<sup>39</sup>, an explicit solution for  $\mathbf{T}$  cannot be exhibited. For this reason we proceed by writing the solution for  $\mathbf{T}$  iteratively, in a series in  $H_I$ : in particular, we use Eq. (31) to determine  $\mathbf{a}$  to first order ( $\mathbf{a}_1$ ) in  $H_I$ . We provide the details in Appendix A and the result for  $\mathbf{a}_1$  in Eq. (A4). Using Eq. (A4) and setting  $\mathbf{T} \approx \mathbf{a}_1$ , we find that Eq. (23) reads

$$\mathbf{S}^\dagger H_{\text{BH}} \mathbf{S} = H_{\text{BH}} + [H_0, \mathbf{a}_1] + [H_I, \mathbf{a}_1]. \quad (33)$$

The GW procedure may be readily iterated to determine, in principle,  $\mathbf{T}$  to any desired order in  $H_I$ . However, since keeping only second-order contributions in  $H_I$  provides

already quite an excellent estimate for the real-space correlation functions of operators in the BH model (as explicitly shown by the numerical calculations we report in Sec. VI), setting  $\mathbf{T} \approx \mathbf{a}_1$  already provides quite a good approximation to the exact  $\mathbf{T}$ .

Since the approach we are implementing is perturbative in  $H_I$ , one should enforce Eq. (31), as well as Eq. (32), to each order in  $H_I$ ; moreover, since  $\mathcal{P}[H_0, \mathbf{a}_1]\mathcal{P} = 0$ , one may neglect the term  $[H_0, \mathbf{a}_1]$  in Eq. (33) and approximate the effective Hamiltonian acting within  $\mathcal{F}$  as

$$H_{\text{eff}} = \mathcal{P} \{H_{\text{BH}} + [H_I, \mathbf{a}_1]\} \mathcal{P} \equiv H_{\text{XXZ}}^{(0)} + H^{(1)}. \quad (34)$$

The first term in the right hand side of Eq. (34) yields a spin-1/2 Hamiltonian which is actually the spin-1/2 XXZ chain introduced in Sec. II B and having the anisotropy and the coupling given by Eqs. (5, 6):

$$H_{\text{XXZ}}^{(0)} \equiv \mathcal{P} H_{\text{BH}} \mathcal{P} = -J \sum_i \left( s_i^x s_{i+1}^x + s_i^y s_{i+1}^y - \frac{V}{J} s_i^z s_{i+1}^z \right) \quad (35)$$

with  $J = 2t \left( f + \frac{1}{2} \right)$  (constant terms have been omitted). The effective spin-1/2 operators are defined as

$$\begin{aligned} s_i^x &= \frac{1}{2\sqrt{f + \frac{1}{2}}} \mathcal{P} \left( b_i + b_i^\dagger \right) \mathcal{P}, \\ s_i^y &= \frac{i}{2\sqrt{f + \frac{1}{2}}} \mathcal{P} \left( -b_i + b_i^\dagger \right) \mathcal{P}, \\ s_i^z &= \mathcal{P} \left( b_i^\dagger b_i - f \right) \mathcal{P}; \end{aligned} \quad (36)$$

the boson number eigenstates at site  $i$  correspond to the eigenstates of  $s_i^z$  according to  $|\bar{n}\rangle_i \leftrightarrow |\downarrow\rangle_i$ , and

$|\bar{n} + 1\rangle_i \leftrightarrow |\uparrow\rangle_i$ . Therefore, the result in Eq. (35) corresponds to the “naive” large- $U$  limit for the BH model at half-integer filling discussed in Sec. II B, in which off-diagonal matrix elements of relevant operators (including the Hamiltonian itself) are set to zero from the very beginning.

Corrections to  $H_{\text{XXZ}}^{(0)}$  arising from virtual transitions involving states outside of  $\mathcal{F}$  may be properly accounted for within GW procedure, allowing to get the effective spin-1/2 Hamiltonian to the next order in  $t/U$ . Summing over all virtual transitions outside of  $\mathcal{F}$  induced by  $H_I$ , one finds

$$\begin{aligned} H^{(1)} \equiv \mathcal{P}[H_I, \mathbf{a}_1]\mathcal{P} &= -t^2 \sum_{j,\ell} \mathcal{P} \left( b_j^\dagger b_{j+1} + b_{j+1}^\dagger b_j \right) \times \\ &\times (\mathbf{I} - \mathcal{P}) (H_{\text{BH}})^{-1} (\mathbf{I} - \mathcal{P}) \left( b_\ell^\dagger b_{\ell+1} + b_{\ell+1}^\dagger b_\ell \right) \mathcal{P}. \end{aligned} \quad (37)$$

In particular, when computing  $H^{(1)}$ , one has to consider intermediate states with either one of the  $\mu_j$  in Eq. (19) being equal to 2, or to  $-1$  (all these states have energy  $\sim U$ , with respect to states in the subspace  $\mathcal{F}$ ), or states with one of the  $\mu_j$  equal to 2 ( $-1$ ), and the other equal to  $-1$  (2) (all these states have energy  $\sim 2U$ , with respect to states in the subspace  $\mathcal{F}$ ). Thus, one eventually finds out that  $H^{(1)}$  can be written as the sum of two terms:  $H^{(1)} = H_{\text{diag}}^{(1)} + H_{\text{offd}}^{(1)}$ , with  $H_{\text{diag}}^{(1)}$  being the part of  $H^{(1)}$  having 1- and 2-nearest-neighbour spin terms, while  $H_{\text{offd}}^{(1)}$  contains 2-next-nearest-neighbour and 3-spin terms. Omitting constant terms, their expression are given by:

$$H_{\text{diag}}^{(1)} = -\frac{4(\bar{n} + 1)t^2}{U} \sum_i s_i^z - \frac{t^2}{U} (3\bar{n}^2 + 6\bar{n} + 4) \sum_i s_i^z s_{i+1}^z \quad (38)$$

$$H_{\text{offd}}^{(1)} = -\frac{t^2(\bar{n} + 1)^2}{U} \sum_i (s_{i+1}^+ s_{i-1}^- + s_{i+1}^- s_{i-1}^+) - \frac{2t^2(\bar{n} + 1)}{U} \sum_i (s_{i+1}^+ s_{i-1}^- + s_{i+1}^- s_{i-1}^+) s_i^z. \quad (39)$$

As we shall see in the next section, using a Luttinger liquid representation,  $H^{(1)}$  may be recast in the XXZ form with coupling and anisotropy coefficients depending on  $U$ .

#### IV. EFFECTIVE XXZ PARAMETERS VIA A LUTTINGER LIQUID REPRESENTATION

The effective spin Hamiltonian in Eq. (34) is not in the XXZ form: in this section we show how the con-

tribution coming from  $H^{(1)}$  may be accounted for by a pertinent redefinition of the parameters of the spin-1/2 XXZ-Hamiltonian  $H_{\text{XXZ}}^{(0)}$ .

The first contribution to  $H_{\text{diag}}^{(1)}$  in the right-hand side of Eq. (38) describes an effective magnetic field in the  $z$  direction<sup>85</sup>, while the second term simply shifts the value of the XXZ anisotropy. At variance, the term  $H_{\text{offd}}^{(1)}$  in Eq. (39) contains 3-spin, as well as non-nearest neighbour, couplings. To show how these terms can be accounted for via a redefinition of  $H_{\text{XXZ}}^{(0)}$ , it is most con-

venient to introduce the Jordan-Wigner (JW) fermions  $a_j, a_j^\dagger$ , in terms of which one gets

$$H_{\text{XXZ}}^{(0)} = -2J \sum_k \cos(k) a_k^\dagger a_k + J\Delta \sum_j :a_j^\dagger a_j: :a_{j+1}^\dagger a_{j+1}:, \quad (40)$$

where  $a_k$  are JW fermionic operators in momentum space and  $::$  denotes normal ordering with respect to the fermionic ground-state. In terms of JW fermions, one writes  $H_{\text{offd}}^{(1)}$  as a sum of a bilinear ( $H_2$ ), plus a quartic ( $H_4$ ) term, that is

$$H_{\text{offd}}^{(1)} \equiv H_2 + H_4,$$

with

$$H_2 = \frac{t^2(\bar{n}+1)}{U} \sum_i \left( a_{i-1}^\dagger a_{i+1} + a_{i+1}^\dagger a_{i-1} \right) \quad (41)$$

$$H_4 = \frac{2t^2(\bar{n}+1)^2}{U} \sum_i :a_i^\dagger a_i: \left( a_{i-1}^\dagger a_{i+1} + a_{i+1}^\dagger a_{i-1} \right) \quad (42)$$

Since  $H_2$  is bilinear in the JW fermions, it merely modifies the single-fermion dispersion relation, yielding the quadratic Hamiltonian in the JW fermions reading

$$H_{\text{XXZ}}^{(0)} + H_2 = \sum_k \left\{ -2J \cos k + \frac{t^2(\bar{n}+1)}{U} \cos(2k) - B \right\} a_k^\dagger a_k, \quad (43)$$

with  $B = 4(\bar{n}+1)t^2/U$ . Setting  $\epsilon(k) = -2J \cos k + \frac{t^2(\bar{n}+1)}{U} \cos(2k) - B$ , one finds that the Fermi points, defined by  $\epsilon(k_F) = 0$ , are given by

$$\cos k_F = \frac{U(\bar{n}+1)}{2J} - \sqrt{\left( \frac{U(\bar{n}+1)}{2J} \right)^2 + \bar{n} + 2}. \quad (44)$$

Upon linearizing the dispersion relation around  $\pm k_F$  and setting  $k = k_F + p$ , one gets

$$\epsilon(\pm k_F + p) \approx \pm J \sin k_F \left[ 1 - \frac{2J}{U(\bar{n}+1)} \cos k_F \right] p. \quad (45)$$

From Eq. (45) one sees that, since  $\cos k_F \neq 0$ ,  $H_2$  implies a nonzero effective magnetic field  $B_{\text{eff}}$ <sup>85</sup>, as well as a redefinition of the Fermi velocity  $v_F$ . This yields a redefined coupling given by  $B_{\text{eff}}/J_{\text{eff}} = -\cos k_F$ . Since

$$B_{\text{eff}} = -J \cos k_F \left( 1 - \frac{2J}{U} \cos k_F \right),$$

one obtains

$$J_{\text{eff}} = J \left( 1 - \frac{2J}{U} \cos k_F \right). \quad (46)$$

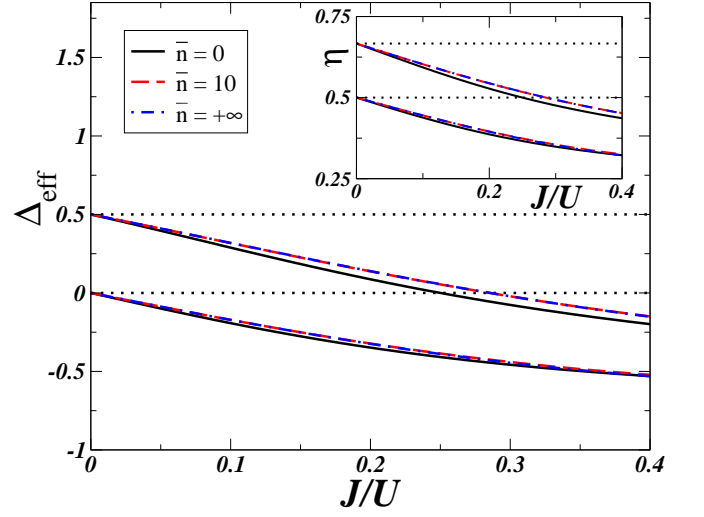


FIG. 1:  $\Delta_{\text{eff}}$  vs.  $J/U$  for different values of  $V/J$  and  $\bar{n}$ . The top (bottom) dotted line corresponds to the value of  $\Delta_{\text{eff}}$  for  $U/J \rightarrow \infty$  and  $V/J = 0.5$  ( $V/J = 0$ ). The other lines are for  $V/J = 0.5$  (top) and  $V/J = 0$  (bottom), with  $\bar{n} = 0$  (solid black lines),  $\bar{n} = 10$  (dashed red lines) and  $\bar{n} \rightarrow \infty$  (dot-dashed blue lines). Inset: same as in the main panel, but for  $\eta$  vs.  $J/U$ .

The quartic term  $H_4$  can be dealt with by noticing that, in the low-energy, long-wavelength limit, one can write

$$a_{j-1}^\dagger a_{j+1} + a_{j+1}^\dagger a_{j-1} \longrightarrow - \left\{ \rho_R(x_j) + \rho_L(x_j) - (-1)^j [\psi_R^\dagger(x_j) \psi_L(x_j) + \psi_L^\dagger(x_j) \psi_R(x_j)] \right\}, \quad (47)$$

where the chiral fermion fields  $\psi_R(x_j), \psi_L(x_j)$  are defined from the long-wavelength expansion of  $a_j$  as

$$a_j \approx e^{ik_F x_j} \psi_R(x_j) + e^{-ik_F x_j} \psi_L(x_j), \quad (48)$$

with  $x_j = aj$ , and the chiral fermion densities given by  $\rho_R(x_j) = \psi_R^\dagger(x_j) \psi_R(x_j)$  and  $\rho_L(x_j) = \psi_L^\dagger(x_j) \psi_L(x_j)$ . As a result,  $H_4$  may be written as

$$H_4 = -\frac{4t^2(\bar{n}+1)^2}{U} \int_0^L dx \left\{ (\rho_R(x))^2 + (\rho_L(x))^2 + 4\rho_R(x)\rho_L(x) \right\}. \quad (49)$$

Comparing Eq. (49) to Eq. (40), one sees that  $H_4$  takes the same form as the term  $J \sum_j s_j^z s_{j+1}^z$  in the spin-1/2 XXZ Hamiltonian in Eq. (4).

Collecting together all the above results allows to write an effective XXZ Hamiltonian, describing the BH model to the order  $(t/U)^2$ , as:

$$H_{\text{XXZ}}^{\text{eff}} = -J_{\text{eff}} \sum_j \left( s_j^x s_{j+1}^x + s_j^y s_{j+1}^y - \Delta_{\text{eff}} s_j^z s_{j+1}^z \right), \quad (50)$$



with  $J_{\text{eff}}$  defined in Eq. (46) and

$$\Delta_{\text{eff}} = \frac{\bar{\Delta}}{1 - \frac{2J}{U} \cos(k_F)} \quad (51)$$

with

$$\bar{\Delta} = \frac{V}{J} - \frac{t^2(3\bar{n}^2 + 6\bar{n} + 4)}{JU} - \frac{4t^2(\bar{n} + 1)^2}{JU}. \quad (52)$$

Since  $J_{\text{eff}}$  acts just as an effective over-all scale of  $H_{\text{XXZ}}^{\text{eff}}$ , then  $\Delta_{\text{eff}}$  is the only parameter determining the behavior of spin-spin correlations in the XXZ model. Substituting Eq. (51) in Eq. (9) one gets

$$\eta = 1 - \frac{1}{\pi} \arccos \Delta_{\text{eff}}, \quad (53)$$

which provides an explicit formula for the effective Luttinger parameter for the BH model at half-integer filling. In Fig. 1 we plot both  $\Delta_{\text{eff}}$  and  $\eta$  versus  $J/U$ , for different values of  $V/J$  and  $\bar{n}$ . One sees that  $\bar{n} = 10$  and  $\bar{n} \rightarrow \infty$  are almost indistinguishable, and that the limit of the quantum phase model for Josephson junction arrays ( $\bar{n} \gg 1$ ) at offset charge  $q = e$  is practically reached at  $\bar{n} \sim 10$ . Furthermore, one sees that the dependence of  $\eta$  upon  $\bar{n}$  is rather small.

From Fig. 1 one also sees that  $\Delta_{\text{eff}}$  may be tuned by varying the ratio  $J/U$ : in particular  $\Delta_{\text{eff}}$  can be different from 0 even if  $V = 0$  (as it is typical for alkali atoms). Fig. 1 also suggests the possibility of describing the whole phase diagram of the XXZ spin-1/2 chain using BH model for a single species of bosons with pertinently chosen parameters, see also Sec. VI<sup>86</sup>.

Finally we notice that, since the sign of  $\Delta_{\text{eff}}$  may be changed by a pertinent choice of  $J/U$  and  $V$ , the Luttinger liquid effectively describing the XXZ-Hamiltonian may be repulsive or attractive. As noticed in the context of 1D Josephson junction arrays<sup>67,68</sup>, the transition between the repulsive and the attractive side may be monitored by inserting a weak link (i.e., a nonmagnetic impurity<sup>79</sup>): it would be then interesting to analyze the effects of a weak link introduced in a bosonic system described by the BH Hamiltonian.

## V. CORRELATION FUNCTIONS

The mapping between  $H_{\text{BH}}$  and  $H_{\text{XXZ}}^{\text{eff}}$  derived in Sec. IV enables to select the ground-states on which to compute the pertinent vacuum expectation values. Indeed if  $|\Phi_0\rangle$  is the ground-state of the BH Hamiltonian given in Eq. (3), and  $|\Psi_0\rangle \equiv \mathbf{S}^\dagger |\Phi_0\rangle$  is the ground-state of  $H_{\text{eff}} = \mathbf{S}^\dagger H_{\text{BH}} \mathbf{S}$ , the GW approach requires

$$\begin{aligned} \langle \Phi_0 | \mathcal{O}_{\text{BH}} [\{b, b^\dagger\}] | \Phi_0 \rangle &= \langle \Psi_0 | \mathbf{S}^\dagger \mathcal{O}_{\text{BH}} [\{b, b^\dagger\}] \mathbf{S} | \Psi_0 \rangle \\ &\equiv \langle \Psi_0 | \mathcal{O}_{\text{XXZ}} [\{s^a\}] | \Psi_0 \rangle, \end{aligned} \quad (54)$$

where  $\mathcal{O}_{\text{BH}} [\{b, b^\dagger\}]$  ( $\mathcal{O}_{\text{XXZ}} [\{s^a\}]$ ) denotes a generic BH (XXZ) operator. Of course, Eq. (54) is exact only if  $\mathbf{S}$  is the exact solution of the GW equation (32): by computing it perturbatively at a given order, one recovers the correspondence between ground-state expectation values of BH and spin-1/2 operators at the chosen order.

In the rest of the paper, we will be interested in correlation functions of the following BH operators:

$$\mathcal{M}_{i,j}^z \equiv (n_i - f)(n_j - f), \quad (55)$$

$$\mathcal{M}_{i,j}^\pm \equiv b_i^\dagger b_j. \quad (56)$$

Using the results of Appendix B one has  $\mathbf{S}^\dagger \mathcal{M}_{i,j}^z \mathbf{S} = \mathcal{M}_{i,j}^z \left[ 1 + \mathcal{O}\left(\frac{t^2 \bar{n}^2}{U^2}\right) \right]$ , so that

$$\langle \Phi_0 | (n_i - f)(n_j - f) | \Phi_0 \rangle = \langle \Psi_0 | s_i^z s_j^z | \Psi_0 \rangle + \mathcal{O}\left(\frac{t^2 \bar{n}^2}{U^2}\right). \quad (57)$$

More generally, if the operator  $\mathcal{O}_{\text{BH}}$  satisfies  $(\mathbf{I} - \mathcal{P}) \mathcal{O}_{\text{BH}} \mathcal{P} = \mathcal{P} \mathcal{O}_{\text{BH}} (\mathbf{I} - \mathcal{P}) = 0$ , then  $\langle \Phi_0 | \mathcal{O}_{\text{BH}} | \Phi_0 \rangle \approx \langle \Psi_0 | \mathcal{O}_{\text{XXZ}} | \Psi_0 \rangle$ , with  $\mathcal{O}_{\text{XXZ}}$  obtained from  $\mathcal{O}_{\text{BH}}$  by substituting  $b_i$ ,  $b_i^\dagger$  and  $n_i - f$  respectively with  $s_i^-$ ,  $s_i^+$  and  $s_i^z$ . At variance, for  $\mathcal{M}_{i,j}^\pm$  one obtains a more involved expression (see Appendix B for details):

$$\begin{aligned} \langle \Phi_0 | b_i^\dagger b_j | \Phi_0 \rangle &\approx (\bar{n} + 1) \langle \Psi_0 | s_i^- s_j^+ | \Psi_0 \rangle + \frac{t(\bar{n} + 2)(\bar{n} + 1)}{2U} \langle \Psi_0 | [s_{i+1}^- + s_{i-1}^-] s_j^+ + [s_{j+1}^+ + s_{j-1}^+] s_i^- | \Psi_0 \rangle \\ &+ \frac{t\bar{n}(\bar{n} + 1)}{2U} \langle \Psi_0 | s_i^- [s_{j-1}^+ + s_{j+1}^+] + s_j^+ [s_{i-1}^- + s_{i+1}^-] | \Psi_0 \rangle + \delta_{|i-j|,1} \langle \Psi_0 | \left( \frac{1}{2} - s_{i+1}^z \right) \left( \frac{1}{2} + s_i^z \right) | \Psi_0 \rangle, \end{aligned} \quad (58)$$

where again we neglected contributions arising to  $\mathcal{O}\left(\frac{t^2 \bar{n}^2}{U^2}\right)$ .

## VI. RESULTS

In this section we compare the numerical results obtained by means of DMRG for the correlation functions

and the phase diagram of the BH model with the analytical predictions for the correlators from the effective Hamiltonian  $H_{\text{XXZ}}^{\text{eff}}$  given by Eq. (50).

### A. Correlation functions

Let us focus on the BH correlation functions. Since DMRG simulations are performed on a finite number of sites  $L$  and for open boundary conditions, we may use Eqs. (14, 15) yielding the  $zz$  and  $xy$  correlation functions of the XXZ model. We evaluate the values of the non-universal constants  $a, b, c$  defined in Eq. (18) both numerically and analytically, by using the expressions presented in Refs. 35,36 and reported in Sec. II B. As confirmed in Ref. 34, the values of  $a, b, c$  obtained in the two ways are in excellent agreement. We show that the analytical expressions for the XXZ correlations are well confirmed by the numerical BH correlations also for small  $L$  (e.g., for  $L = 30$ ) and for  $J/U$  relatively large (as large as  $\sim 0.5$ ). It should be stressed that, at variance, the agreement is not very good by setting  $\Delta_{\text{eff}} = V/J$ , i.e. by using the Hamiltonian  $H_{\text{XXZ}}^{(0)}$  obtained for  $U \rightarrow \infty$  neglecting contributions arising from the GW procedure.

The correlators  $\langle \Phi_0 | (n_i - f)(n_j - f) | \Phi_0 \rangle$  and  $\langle \Phi_0 | b_i^\dagger b_j | \Phi_0 \rangle$  are evaluated from the corresponding XXZ quantities using respectively Eqs. (57) and (58). They are plotted in Figs. 2-9 as a function of  $r = |i - j|$ , with  $i$  and  $j$  such that<sup>34</sup>  $i = (L - r + 1)/2$ ,  $j = (L + r + 1)/2$  for odd  $r$ , and  $i = (L - r)/2$ ,  $j = (L + r)/2$  for even  $r$  (for instance, for  $L = 100$  sites,  $r = 1$  corresponds to  $i = 50$ ,  $j = 51$ ;  $r = 2$  corresponds to  $i = 49$ ,  $j = 51$ ;  $r = 3$  corresponds to  $i = 49$ ,  $j = 52$ , and so on). The meaning of the various symbols is summarized in the following table:

filled squares (black)	numerical BH results
filled diamonds (green)	XXZ results - analytical $a, b, c$
filled triangles (red)	XXZ results - numerical $a, b, c$
stars (blue)	infinite- $U$ results
open circles (magenta)	non-rotated operators

In Fig. 2 we plot our results for the density-density correlations  $\langle (n_i - f)(n_j - f) \rangle$  for a typical set of values, i.e. for  $U = 10t$ ,  $V = 0.5t$ ,  $f = 0.5$ , corresponding to  $J/U = 0.2$ . Black squares (joint by a black line as a guide for eye) are the density-density correlations evaluated in the BH model, red triangles (line) are the correlation functions  $\langle s_i^z s_j^z \rangle$  in the ground-state of the XXZ chain with effective anisotropy given by Eq. (51) and the  $a, b, c$  constants numerically determined from DMRG simulations of the XXZ chain, while the green diamonds (line) correspond to  $a, b, c$  analytically determined from Eqs. (18) and (10, 11, 12). We found that, up to numerical accuracy  $\lesssim 10^{-5}$ , results obtained analytically for the XXZ effective model are in excellent agreement with results of the density-density BH model even at small distance. Blue stars (line) display the XXZ Hamiltonian

results in the  $U \rightarrow \infty$  limit, with anisotropy  $\Delta = V/J$  – in that case the relative error is noticeably larger.

In Fig. 3 we plot the off-diagonal correlations  $\langle b_i^\dagger b_j \rangle$  for the same set of values of the BH parameters as in Fig. 2. Also here one sees that the results obtained from the GW effective Hamiltonian  $H_{\text{XXZ}}^{\text{eff}}$  are in much better agreement than the ones obtained using  $H_{\text{XXZ}}$  with  $\Delta = V/J$ , this happens even though  $J/U$  is as low as 0.2.

To quantify the agreement between BH and XXZ results, we consider the absolute value of the relative error done in evaluating a correlator  $\mathcal{C}(r)$  as the ground-state average of the corresponding operators in the BH model [ $\mathcal{C}_{\text{BH}}(r)$ ], and in the XXZ model [ $\mathcal{C}_{\text{XXZ}}(r)$ ]. More precisely, we define

$$\delta\mathcal{C}(r) = \left| \frac{\mathcal{C}_{\text{BH}}(r) - \mathcal{C}_{\text{XXZ}}(r)}{\mathcal{C}_{\text{BH}}(r)} \right| \quad (59)$$

focusing on  $\mathcal{C}_{zz}(r) \equiv |\langle (n_i - f)(n_j - f) \rangle|$  and  $\mathcal{C}_{xy}(r) \equiv \text{Re}[\langle b_i^\dagger b_j \rangle]$ . To summarize the information on the relative error, we compute the average value  $\delta_{\text{av}}\mathcal{C}$  and the standard deviation of the relative error (59) for a distance  $r = |i - j|$  between a minimum value  $r_{\text{min}} = 1$  (2) for  $zz$  ( $xy$ ) correlations, and a maximum value  $r_{\text{max}} \sim 3L/5$ .

The relative errors for the  $zz$  and  $xy$  correlation functions are plotted in Figs. 4-5: the error made using the GW  $H_{\text{XXZ}}^{\text{eff}}$  is of the order of few percents (in agreement with  $(J/U)^2 = 0.04$ ). At variance, the relative error made by using the XXZ model in the infinite- $U$  limit without applying the GW procedure is much larger, although the value of  $J/U$  is not so large. Indeed, the error  $\delta_{\text{av}}$  is

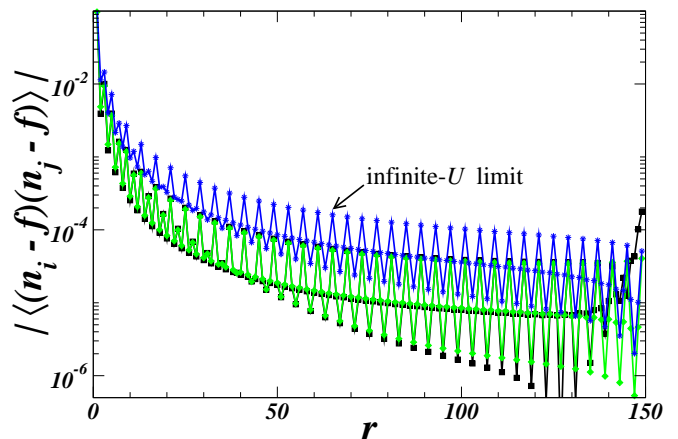


FIG. 2: Density-density correlations  $|\langle (n_i - f)(n_j - f) \rangle|$  vs.  $r = |i - j|$  for  $U = 10t$ ,  $V = 0.5t$  and  $f = 0.5$ , with number of sites  $L = 150$ . Black squares: numerical BH results; green diamonds: XXZ result with  $a, b, c$  analytically determined; blue stars:  $U \rightarrow \infty$  XXZ result (indicated by the label “infinite- $U$  limit” – see text for further details). Lines are guide for eye. On the scale of the figure, results obtained for the XXZ model with  $a, b, c$  numerically determined (not shown here) are indistinguishable from the ones obtained with the corresponding analytical values. Notice also the excellent agreement between numerical BH findings and analytical XXZ results.

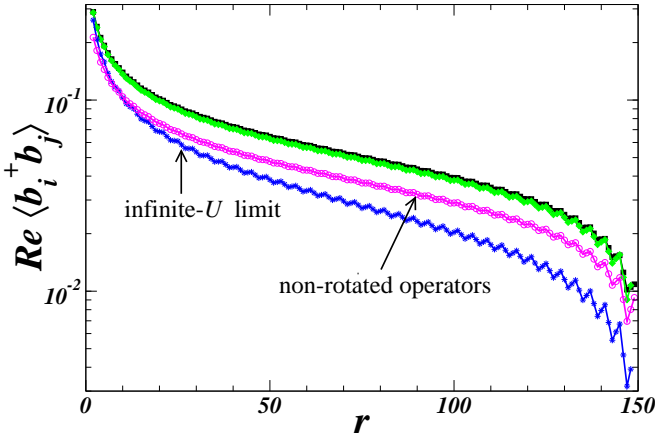


FIG. 3: Real part of  $\langle b_i^\dagger b_j \rangle$  vs.  $r = |i - j|$  for  $U = 10t$ ,  $V = 0.5t$ ,  $f = 0.5$ ,  $L = 150$ . Magenta circles denote XXZ results with “non-rotated operators”. The notation for the other symbols is the same as in Fig. 2.

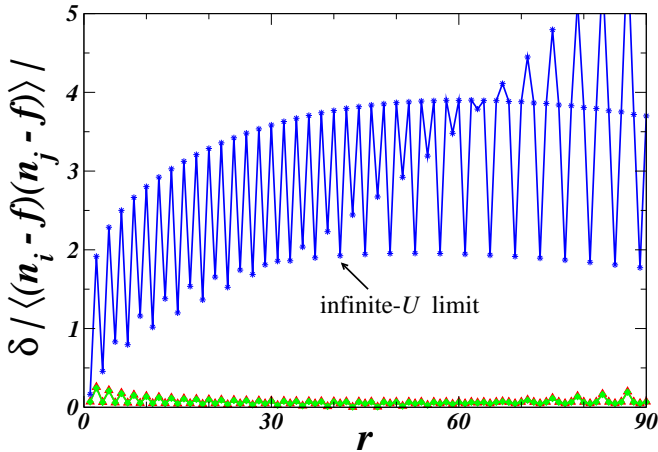


FIG. 4: Relative error of the correlation function  $|\langle (n_i - f)(n_j - f) \rangle|$  vs.  $r = |i - j|$  for the same parameters (and the same conventions for symbols and lines) of Fig. 2. We also plot the results obtained from the XXZ model with  $a, b, c$  numerically determined as red triangles: numerical and analytical estimates for finite  $U$  practically coincide. The average value, with  $r_{\max} = 3L/5$ , is  $0.06 \pm 0.04$  for the finite- $U$  XXZ model and  $2.9 \pm 1.2$  for the infinite- $U$  XXZ model.

$\sim 300\%$  for the  $zz$  correlations and  $\sim 40\%$  for the  $xy$  correlations (to be compared with  $\sim 6\%$  and  $\sim 3\%$  obtained from  $H_{\text{XXZ}}^{\text{eff}}$ ). We checked that these results do not depend on the particular choice of  $r_{\max}$ : of course, when  $r_{\max}$  is closer to  $L$ , the error is larger (especially for the density-density correlations) due to boundary effects. From the data of Figs. 4-5, one also sees that, at short distance, it is larger than that at intermediate distances (with  $r$  being few units it is  $\lesssim 10\%$ ). As expected, it decreases at the center of the chain  $r \sim L/2$ , while, close to the end of the chain  $r \sim L$ , it increases. We also observe that finite-size effects are less visible for  $xy$  correlations.

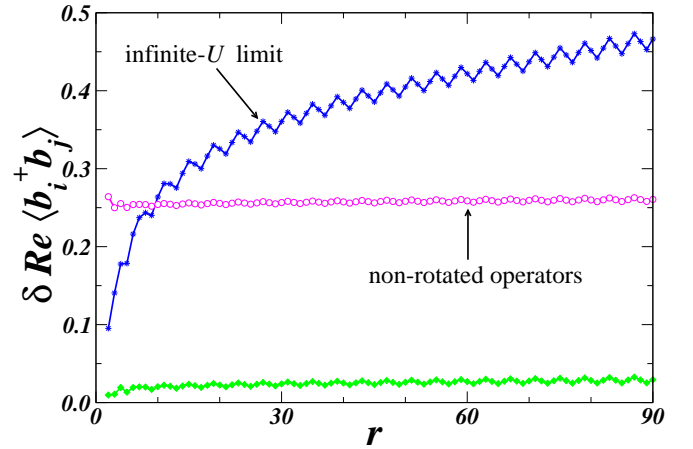


FIG. 5: Relative error of the real part of  $\langle b_i^\dagger b_j \rangle$  vs.  $r = |i - j|$  for the same parameters (and the same conventions for symbols and lines) of Fig. 3. The average values, with  $r_{\max} = 3L/5$ , are:  $0.025 \pm 0.004$  (green diamonds - analytical XXZ results),  $0.38 \pm 0.08$  (blue stars - XXZ result in the infinite- $U$  limit),  $0.26 \pm 0.03$  (magenta circles - finite- $U$  result with non-rotated operators).

The agreement between numerical and analytical results turns out to be stable also if one takes chains with smaller sizes, as it is apparent from Figs. 6-7, where we plot the  $zz$  and  $xy$  correlation functions for different  $L$ . The corresponding errors are given in the following table:

$L$	$\delta_{\text{av}}^{(U)} \mathcal{C}_{zz}$	$\delta_{\text{av}}^{(\infty)} \mathcal{C}_{zz}$	$\delta_{\text{av}}^{(U)} \mathcal{C}_{xy}$	$\delta_{\text{av}}^{(\infty)} \mathcal{C}_{xy}$
30	$0.12 \pm 0.08$	$1.7 \pm 0.9$	$0.04 \pm 0.01$	$0.26 \pm 0.07$
50	$0.10 \pm 0.06$	$2.0 \pm 1.0$	$0.04 \pm 0.01$	$0.29 \pm 0.08$
80	$0.09 \pm 0.05$	$2.4 \pm 1.0$	$0.04 \pm 0.01$	$0.33 \pm 0.08$
100	$0.08 \pm 0.05$	$2.5 \pm 1.1$	$0.04 \pm 0.01$	$0.35 \pm 0.08$
150	$0.07 \pm 0.04$	$2.9 \pm 1.2$	$0.04 \pm 0.01$	$0.38 \pm 0.08$

where for simplicity  $\delta_{\text{av}}^{(U)}$  ( $\delta_{\text{av}}^{(\infty)}$ ) denotes the average error for the XXZ correlators at finite- $U$  (infinite- $U$  limit) with (without) the GW procedure. We see that, for the density-density  $zz$  correlations, the average error increases when the size  $L$  decreases.

In Figs. 3 and 5 we also plotted (magenta circles and lines) the results obtained according to Eq. (54), where we took  $\mathcal{O}_{\text{XXZ}} = \mathcal{O}_{\text{BH}}$  and not  $\mathcal{O}_{\text{XXZ}} = \mathbf{S}^\dagger \mathcal{O}_{\text{BH}} \mathbf{S}$ . Indeed, as stressed in Ref. 87, solving the equation for  $\mathbf{S}$  amounts to perturbatively find a transformation enabling to block-diagonalize  $H_{\text{BH}}$ . The ground-state of  $H_{\text{BH}}$  changes accordingly: if one wants to compute expectation values of certain operators in the BH model, one has to rotate the chosen operator according the  $\mathbf{S}$  transformation - in other words, physical quantities in the effective theory are not simply the expectation values of the operators in the projected subspace: this guarantees the unitarity of the procedure. An example is already provided in Ref. 43 for the computation of the staggered magnetization in the 2D Fermi-Hubbard model with large- $U$  effective spin models. In Appendix B we give details on the the explicit

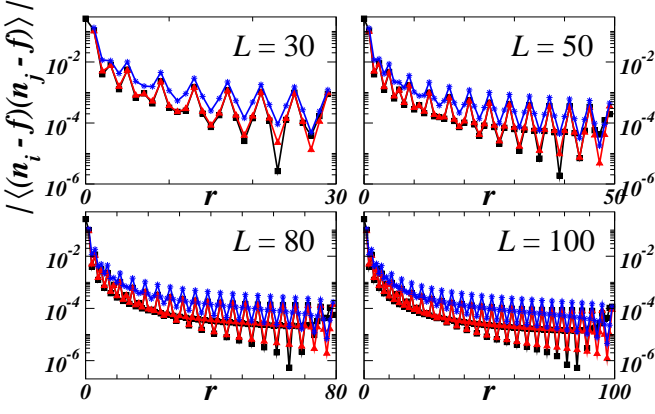


FIG. 6: In each panel we plot  $|\langle(n_i - f)(n_j - f)\rangle|$  vs.  $r = |i - j|$  for different sizes:  $L = 30, 50, 80, 100$  ( $U = 10t$ ,  $V = 0.5t$ ,  $f = 0.5$ ). Black squares denote the BH results, red triangles the XXZ results with  $a, b, c$  numerically determined, and blue stars the infinite- $U$  XXZ results (we do not report the XXZ results with  $a, b, c$  analytically determined, since they practically coincide with the red triangles).

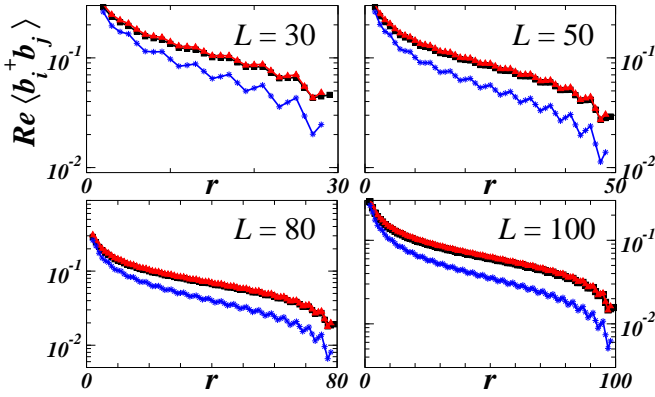


FIG. 7: Real part of  $\langle\hat{b}_i^\dagger \hat{b}_j\rangle$  vs.  $r = |i - j|$  for the sizes and the parameters of Fig. 6.

computation of the GW rotation for the operators  $b_i^\dagger b_j$  and  $(n_i - f)(n_j - f)$ . We remark that, while for density-density correlation functions ( $zz$  correlations in the XXZ model) magenta circles coincide with black squares, this is not the case for  $\langle\hat{b}_i^\dagger \hat{b}_j\rangle$  ( $xy$  planar correlations in the XXZ model).

In Figs. 8-9 we plot the  $zz$  and  $xy$  correlation functions for different values of  $U$ : in these plots the ratio  $J/U$  ranges from 0.1 to 0.6. As expected, one sees that for  $J/U = 0.1$  the relative error made by the infinite- $U$  results is not very large ( $\sim 10\%$  for  $\langle\hat{b}_i^\dagger \hat{b}_j\rangle$  correlations), but, as soon as  $J/U \gtrsim 0.2$ , it is already well visible. The relative error made by using the effective  $H_{\text{XXZ}}^{\text{eff}}$  turns out to be rather small even for  $J/U = 0.6$ , where the relative error on density-density correlations is only  $\approx 7\%$ , while for  $\langle\hat{b}_i^\dagger \hat{b}_j\rangle$  correlations it is  $\approx 15\%$ <sup>88</sup>.

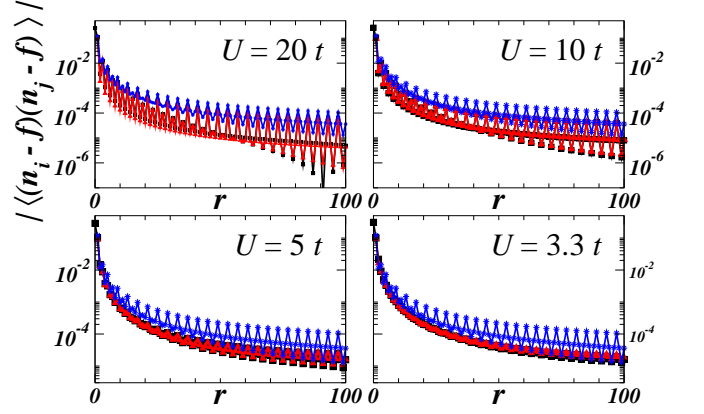


FIG. 8: Density-density correlations  $|\langle(n_i - f)(n_j - f)\rangle|$  vs.  $r = |i - j|$  for different values of  $U/t = 20, 10, 5, 3.3$ , corresponding, respectively, to  $J/U = 0.1, 0.2, 0.4, 0.6$  (with  $V = 0.5t$ ,  $f = 0.5$ ,  $L = 150$ ).

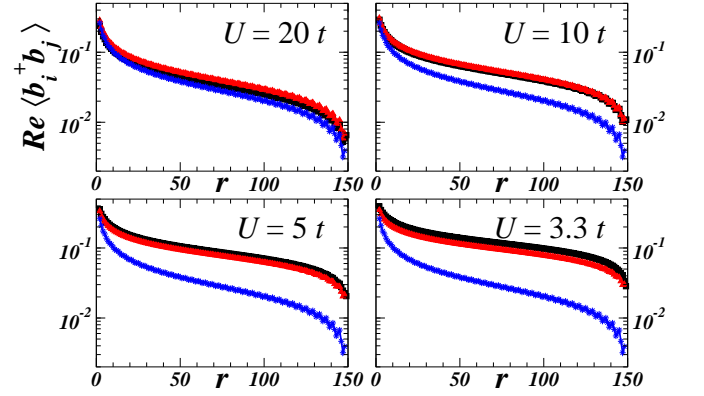


FIG. 9: Real part of  $\langle\hat{b}_i^\dagger \hat{b}_j\rangle$  vs.  $r = |i - j|$  for the  $U$  values and the parameters of Fig. 8.

## B. Antiferromagnet and domain ferromagnet in the 1D Bose-Hubbard model

The XXZ model is gapless and critical for  $-1 \leq \Delta \leq 1$ , antiferromagnetic for  $\Delta > 1$  and ferromagnetic for  $\Delta < -1$ : in the latter ferromagnetic phase, all the spins are aligned. However, the BH at half-integer filling maps into the effective XXZ chain (50) supplemented by the condition that the total spin is vanishing: therefore we expect that, in the BH model at  $\Delta_{\text{eff}} < -1$ , domain walls form separating regions with “up” spins (i.e. with  $f + 1/2$  particles per site) and regions with “down” spins (i.e., with  $f - 1/2$  particles per site). At variance, at  $\Delta_{\text{eff}} > 1$  the staggered magnetization becomes non vanishing: in the bosonic BH language the antiferromagnetic state corresponds to the “charge-checkboard ordered state”  $|f + 1/2, f - 1/2, f + 1/2, f - 1/2, \dots\rangle$ .

This shows that, consistently with the XXZ representation of the BH model at half-integer filling, at finite  $U$  one can realize the transition between the spin-liquid and the Néel-Ising antiferromagnetic phase of the XXZ model

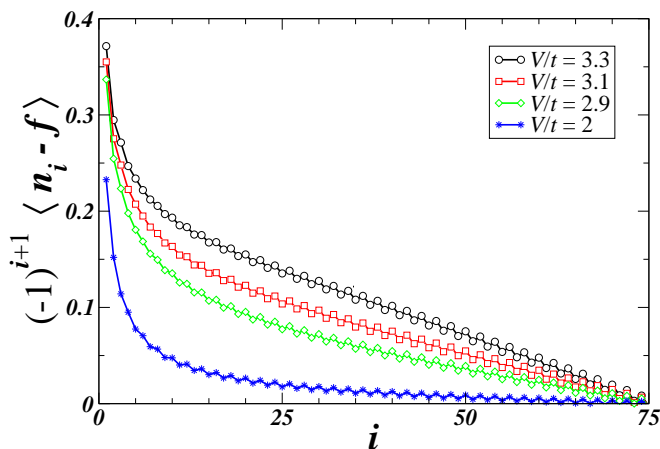


FIG. 10: Plot of  $(-1)^{i+1} \langle n_i - f \rangle$  vs.  $i$  numerically computed in the BH chain for  $U = 10t$ ,  $f = 0.5$  and  $L = 150$  for different values of  $V$ : from top to bottom  $V/t = 3.3$  (black circles),  $V/t = 3.1$  (red squares),  $V/t = 2.9$  (green diamonds) and  $V/t = 2$  (blue stars) corresponding, respectively, to  $\Delta_{\text{eff}} = 1.09, 1.00, 0.91, 0.52$ .

(superfluid to charge-density-wave phase transition of the BH model), as well as the transition between the spin-liquid and the domain ferromagnetic phase of the XXZ model (superfluid to domain Mott-insulating phase transition of the BH model)<sup>86</sup>. Since the former transition sets in at  $\Delta_{\text{eff}} = 1$  and the latter one at  $\Delta_{\text{eff}} = -1$ , using Eq. (51) for  $\Delta_{\text{eff}}$  allows to determine the corresponding phase boundaries in terms of the parameters of the BH Hamiltonian.

A complete discussion of the phase diagram of the BH chain in presence of nearest-neighbour interactions is provided in Ref. 58: here we just focus on the half-integer BH chain with parameters chosen so as to lie close to  $\Delta_{\text{eff}} = \pm 1$ , in order to show that the effective XXZ representation given in this paper also provides a good description of these transitions.

For the spin-liquid/ferromagnetic transition, we studied the BH chain with open boundary conditions varying  $V$  (similar results are obtained varying  $t$ ) and we plot in Fig. 10 the expectation value of  $(n_i - f)$  as a function of the position  $i$  along the chain. We observe that, as a consequence of the open boundary conditions, a magnetic field proportional to  $V$  on the two boundaries (i.e., at  $i = 1$  and  $i = L$ ) appears, whose effect close to the boundaries is clearly visible in the figure. Computing the quantity  $\mathcal{N} = \sum_r (-1)^{i-j} \langle (n_i - f)(n_j - f) \rangle$ , one sees that it significantly increases around a critical value  $\Delta_{\text{eff}}^{AF}$ . From the numerical data for the BH model shown in Fig. 10 one may estimate  $\Delta_{\text{eff}}^{AF} \sim 1.05$ , in good agreement with the analytical value  $\Delta_{\text{eff}}^{AF} = 1$ <sup>89</sup>. We notice that a better estimate of  $\Delta_{\text{eff}}^{AF}$  could be performed by adding a magnetic field in the boundaries to compensate the boundary magnetic fields arising from the open boundary conditions.

Regarding the domain ferromagnet/superfluid transi-

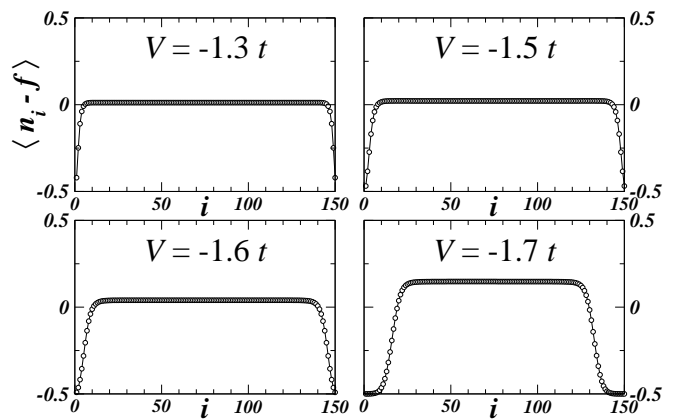


FIG. 11: Plot of  $\langle n_i - f \rangle$  vs.  $i$  numerically computed in the BH chain for  $U = 10t$ ,  $f = 0.5$  and  $L = 150$  for different values of  $V$ :  $V/t = -1.3, -1.5, -1.6, -1.7$ , corresponding, respectively, to  $\Delta_{\text{eff}} = -0.91, -1.00, -1.04, -1.08$ .

tion, we performed numerical simulations on the BH model with parameters chosen such that  $\Delta_{\text{eff}}$  is close to  $-1$  (see Figs. 11-12). In Fig. 11 we plot  $\langle n_i - f \rangle$  as a function of the position  $i$ : one sees that the expectation value of the spin is constant and it changes sign close to the edges of the chain in order to satisfy the constraint on the number conservation. For this reason we then plot the modulus of the same quantity in Fig. 12: since the average of the  $s_z^i$  expectation values is of course zero, to determine the transition point from BH numerical data we consider the averaged quantity  $\sum_{i=1}^L |\langle n_i - f \rangle|$  (e.g., for the different values of  $V$  shown in Fig. 12, such quantity is reported in the caption). From these data one can estimate that the domain ferromagnet is occurring at  $\Delta_{\text{eff}}^F \sim -1.02$ , with an error of few percent with respect to the analytical result  $\Delta_{\text{eff}}^F = -1$ <sup>89</sup>. Notice that the error made by using  $H_{\text{XXZ}}$  with  $\Delta = V/J$  in the infinite- $U$  limit is  $\approx 20\%$ : as expected, the errors made in using the infinite- $U$  results are generally smaller when one deals with global quantities.

## VII. CONCLUDING REMARKS

In this paper we studied an XXZ representation of the Bose-Hubbard chain at half-integer filling for finite on-site interaction energy  $U$ . The effective XXZ model is obtained in two steps: first, we used a similarity renormalization group procedure amounting to solve perturbatively up to the order  $(t/U)^2$  the exact equation for the operator block-diagonalizing the Bose-Hubbard model. The resulting spin-1/2 effective Hamiltonian is then recast as a XXZ spin-1/2 Hamiltonian with pertinently redefined coupling and anisotropy parameters.

We use this mapping to provide analytical estimates of the correlation functions of the Bose-Hubbard model at half-integer filling and finite  $U$ . We then compared these analytical results with the outcomes of the numer-

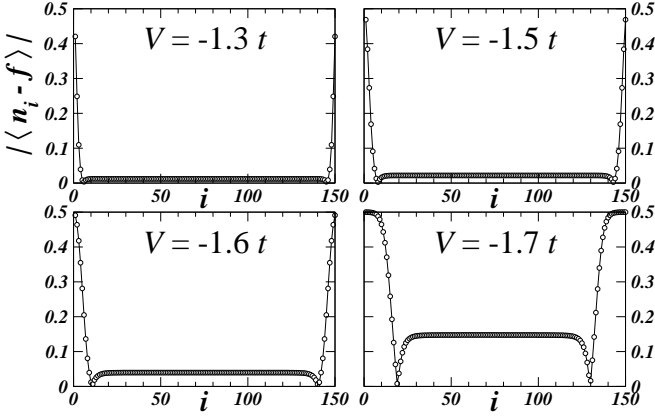


FIG. 12: Plot of the modulus of  $\langle n_i - f \rangle$  vs.  $i$  computed in the BH chain for the same parameters of Fig. 11:  $V/t = -1.3, -1.5, -1.6, -1.7$ . The corresponding averages are  $\approx 0.02, 0.04, 0.06, 0.21$ .

ical DMRG evaluation of the Bose-Hubbard correlation functions. We found that the agreement is very good, also for  $J/U$  rather large ( $\sim 0.5$ ) and for small number of sizes ( $L \sim 30$ ). Such a good agreement is not achieved, even for  $J/U$  relatively small ( $\sim 0.1$ ), if one uses the XXZ Hamiltonian  $H_{\text{XXZ}}^{(0)}$  with  $J = 2t(f + 1/2)$  and  $\Delta = V/J$  corresponding to the infinite-coupling limit of the Bose-Hubbard model. The transitions predicted at  $\Delta_{\text{eff}} = \pm 1$  for the XXZ chain are as well compared with Bose-Hubbard results, and a good agreement is found.

Since the BH model at half-integer filling is not integrable or exactly solvable, it is quite valuable to have analytical estimates for its correlation functions. Besides its mathematical interest, we stress out that our results can be viewed from a two-fold point of view: on one side, we use known results from the (integrable) XXZ model to construct with high accuracy correlation functions of the Bose-Hubbard model. On the other side, the Bose-Hubbard chain at half-filling and at finite  $U$  may be seen as a quantum simulator of the XXZ chain. Finally, our results could be relevant towards extending to the BH model the analysis of nonequilibrium steady state in the XXZ chain performed in Ref. 90.

In our approach, the effect of an harmonic trap results in a locally varying magnetic field: we feel that it would be interesting to compare the results stemming from an XXZ-based approach with the ones known in literature for hard- and soft-core bosons in harmonic traps in the scaling limit<sup>91</sup>. In this paper we focused on the half-integer filling Bose-Hubbard model, but deviations from such filling could be easily accounted with the introduction of a magnetic field. We stress that the similarity Hamiltonian renormalization procedure could also be applied to bosonic ladders<sup>92</sup> and at integer filling, where a spin-1 model is found in the infinite- $U$  limit.

The large- $V$  effects of edge magnetic field could also be studied, following the results known for the XXZ chain<sup>93</sup>: we observe that, for open boundary conditions and finite

$V$ , two boundary magnetic field terms  $-B_b(s_1^z + s_L^z)$ , with  $B_b \propto V$ , emerge in the XXZ effective Hamiltonian<sup>94</sup>. Since a magnetic field at the edge induces corrections to the average value of  $s_i^z$  decreasing as a power law<sup>93</sup>, these corrections are not only expected, but could be also worth the effort of future investigation.

### Acknowledgments

We would like to thank F. Becca, L. Campos-Venuti, F. Essler, A. Ferraz, V. Korepin, F. Minardi, M. Müller, G. Santoro and A. Smerzi for very useful discussions. A.T. acknowledges kind hospitality from IIP-UFRN (Natal), where part of this work was performed. D.R. acknowledges financial support from EU through the project SOLID.

### Appendix A: Perturbative solution of the GW equation

In this Appendix we show how use Eq. (31) to determine  $\mathbf{a}$  to *first order* in  $H_I$ , that is  $\mathbf{a}_1$ . To this order, one gets

$$\mathcal{P} \{H_I + [H_0, \mathbf{a}_1]\} (\mathbf{I} - \mathcal{P}) = 0, \quad (\text{A1})$$

which may be solved by setting

$$\begin{aligned} \mathcal{P} \mathbf{a}_1 (\mathbf{I} - \mathcal{P}) = & \\ \mathcal{P} H_I (\mathbf{I} - \mathcal{P}) \{ & -\mathcal{P} H_0 \mathcal{P} + (\mathbf{I} - \mathcal{P}) H_0 (\mathbf{I} - \mathcal{P}) \}^{-1} \\ & + [\mathcal{P} H_0 \mathcal{P}, \mathcal{P} \mathbf{a}_1 (\mathbf{I} - \mathcal{P})] \\ & \times \{ -\mathcal{P} H_0 \mathcal{P} + (\mathbf{I} - \mathcal{P}) H_0 (\mathbf{I} - \mathcal{P}) \}^{-1}. \end{aligned} \quad (\text{A2})$$

Up to term that are second order in  $t\bar{n}/U$ , we may make the approximation  $\mathcal{P} H_0 \mathcal{P} \approx \mathcal{E}_0[\bar{n}] \mathbf{I}$ , with  $\mathcal{E}_0[\bar{n}] = L \{ \frac{U}{2} \bar{n}(\bar{n} - 1) + V \bar{n}^2 \}$ , which implies  $[\mathcal{P} H_0 \mathcal{P}, \mathcal{P} \mathbf{a}_1 (\mathbf{I} - \mathcal{P})] = 0$ . As a result, we get

$$\begin{aligned} \mathcal{P} \mathbf{a}_1 (\mathbf{I} - \mathcal{P}) = & \mathcal{P} H_I (\mathbf{I} - \mathcal{P}) \\ & \times \{ -\mathcal{P} H_0 \mathcal{P} + (\mathbf{I} - \mathcal{P}) H_0 (\mathbf{I} - \mathcal{P}) \}^{-1}. \end{aligned} \quad (\text{A3})$$

Using the fact that  $\mathbf{a}$  is antihermitean, from Eq. (A3) one obtains

$$\begin{aligned} \mathbf{a}_1 = & \mathcal{P} H_I (\mathbf{I} - \mathcal{P}) \\ & \times \{ -\mathcal{P} H_0 \mathcal{P} + (\mathbf{I} - \mathcal{P}) H_0 (\mathbf{I} - \mathcal{P}) \}^{-1} - \\ & \{ -\mathcal{P} H_0 \mathcal{P} + (\mathbf{I} - \mathcal{P}) H_0 (\mathbf{I} - \mathcal{P}) \}^{-1} \\ & \times (\mathbf{I} - \mathcal{P}) H_I \mathcal{P}. \end{aligned} \quad (\text{A4})$$

### Appendix B: GW transformation of operators

An advantage of the GW procedure is that it may be easily applied to single-boson operators: in particular, we

are interested in the average values of the operators  $\mathcal{M}_{i,j}^\perp$  and  $\mathcal{M}_{i,j}^z$ , defined in Eqs. (55) and (56). Since  $\mathbf{a}_1$  is fully off-diagonal and  $\mathcal{P}\mathcal{M}_{i,j}^z(\mathbf{I} - \mathcal{P}) = 0$ , if one approximates  $\mathbf{T}$  with  $\mathbf{a}_1$ , one obtains  $\mathbf{S}^\dagger \mathcal{M}_{i,j}^z \mathbf{S} = \mathcal{M}_{i,j}^z$ . Instead, acting

onto  $\mathcal{M}_{i,j}^\perp$ , gives raise to a more complicated expression: expressing the final result in terms of spin-1/2 variables, one obtains

$$\begin{aligned} \mathcal{P}\mathbf{S}^\dagger \mathcal{M}_{i,j}^\perp \mathbf{S}\mathcal{P} &\approx \delta_{|i-j|,1} \frac{t\bar{n}(\bar{n}+2)}{U} \left( \frac{1}{2} - s_{i+1}^z \right) \left( \frac{1}{2} + s_i^z \right) \\ &+ \frac{t(\bar{n}+2)(\bar{n}+1)}{U} \left\{ s_{i+1}^- s_j^+ \left( \frac{1}{2} + s_i^z \right) + s_{i-1}^- s_j^+ \left( \frac{1}{2} + s_i^z \right) + s_i^- s_{j+1}^+ \left( \frac{1}{2} + s_j^z \right) + s_i^- s_{j-1}^+ \left( \frac{1}{2} + s_j^z \right) \right\} \\ &+ \frac{t(\bar{n}+2)(\bar{n}+1)}{2U} \left\{ s_i^- s_{j-1}^+ \left( \frac{1}{2} - s_i^z \right) + s_i^- s_{j+1}^+ \left( \frac{1}{2} - s_i^z \right) + s_{i-1}^- s_j^+ \left( \frac{1}{2} - s_j^z \right) + s_{i+1}^- s_j^+ \left( \frac{1}{2} - s_j^z \right) \right\}. \end{aligned} \quad (\text{B1})$$

We observe that due to the constraint on the fixed total particle number  $N$ , the total magnetization in any of the physical states of  $H_{\text{eff}} = H_{\text{XXZ}}^{(0)} + H_{\text{diag}}^{(1)} + H_{\text{offd}}^{(1)}$  is zero: since  $H_{\text{eff}}$  contains no terms breaking the parity symmetry ( $s_i^\alpha \rightarrow -s_i^\alpha$ ), its ground-state  $|\Psi_0\rangle$  is nondegenerate and, thus, it must be parity invariant. As a consequence,

the average of any product of three spin-1/2 operators must necessarily give 0, greatly simplifying the calculation of the ground-state average of the operator.

Using this result one can obtain a simplified expression for  $\langle \Phi_0 | \mathcal{M}_{i,j}^\perp | \Phi_0 \rangle$  at  $\mathcal{O}\left(\frac{t^2 \bar{n}^2}{U^2}\right)$ :

$$\begin{aligned} \langle \Phi_0 | \mathcal{M}_{i,j}^\perp | \Phi_0 \rangle &\approx \delta_{|i-j|,1} \langle \Psi_0 | \left( \frac{1}{2} - s_{i+1}^z \right) \left( \frac{1}{2} + s_i^z \right) | \Psi_0 \rangle \\ &+ \frac{t(\bar{n}+2)(\bar{n}+1)}{U} \langle \Psi_0 | \left\{ s_{i+1}^- s_j^+ \left( \frac{1}{2} + s_i^z \right) + s_{i-1}^- s_j^+ \left( \frac{1}{2} + s_i^z \right) + s_i^- s_{j+1}^+ \left( \frac{1}{2} + s_j^z \right) + s_i^- s_{j-1}^+ \left( \frac{1}{2} + s_j^z \right) \right\} \mathcal{P} | \Psi_0 \rangle \\ &+ \frac{t\bar{n}(\bar{n}+1)}{U} \langle \Psi_0 | \mathcal{P} \left\{ s_i^- s_{j-1}^+ \left( \frac{1}{2} - s_i^z \right) + s_i^- s_{j+1}^+ \left( \frac{1}{2} - s_i^z \right) + s_{i-1}^- s_j^+ \left( \frac{1}{2} - s_j^z \right) + s_{i+1}^- s_j^+ \left( \frac{1}{2} - s_j^z \right) \right\} \mathcal{P} | \Psi_0 \rangle \end{aligned} \quad (\text{B2})$$

Since any product of three spin-1/2 operators must necessarily give 0, then Eq. (B2) gives Eq. (58) reported in

the main text.

<sup>1</sup> S. Blundell, *Magnetism in condensed matter* (Oxford, Oxford University Press, 2001).

<sup>2</sup> *Introduction to frustrated magnetism: materials, experiments, theory*, eds. C. Lacroix, P. Mendels, and F. Mila (Heidelberg, Springer, 2011).

<sup>3</sup> G.B. Jo, Y.R. Lee, J.H. Choi, C.A. Christensen, T.H. Kim, J.H. Thywissen, D.E. Pritchard, and W. Ketterle, *Science* **325**, 1521 (2009).

<sup>4</sup> K. Kim, M.S. Chang, S. Korenblit, R. Islam, E.E. Edwards, J.K. Freericks, G.D. Lin, L.-M. Duan, and C. Monroe, *Nature* **465**, 590 (2010).

<sup>5</sup> S. Fölling, S. Trotzky, P. Cheinet, M. Feld, R. Saers, A. Widera, T. Müller, and I. Bloch, *Nature* **448**, 1029 (2007).

<sup>6</sup> A. Eckardt, C. Weiss, and M. Holthaus, *Phys. Rev. Lett.* **95**, 260404 (2005).

<sup>7</sup> J. Struck, C. Olschlager, R. Le Targat, P. Soltan-Panahi,

A. Eckardt, M. Lewenstein, P. Windpassinger, and K. Senstock, *Science* **333**, 996 (2011).

<sup>8</sup> L.-M. Duan, E. Demler, and M.D. Lukin, *Phys. Rev. Lett.* **91**, 090402 (2003).

<sup>9</sup> G. Thalhammer, G. Barontini, L. De Sarlo, J. Catani, F. Minardi, and M. Inguscio, *Phys. Rev. Lett.* **100**, 210402 (2008).

<sup>10</sup> A.B. Kuklov and B.V. Svistunov, *Phys. Rev. Lett.* **90**, 100401 (2003).

<sup>11</sup> I. Bloch, J. Dalibard, and W. Zwerger, *Rev. Mod. Phys.* **80**, 885 (2008).

<sup>12</sup> D. Jaksch, C. Bruder, J.I. Cirac, C.W. Gardiner, and P. Zoller, *Phys. Rev. Lett.* **81**, 3108 (1998).

<sup>13</sup> J.J. García-Ripoll, M.A. Martin-Delgado, and J.I. Cirac, *Phys. Rev. Lett.* **93**, 250405 (2004).

<sup>14</sup> S. Sachdev, K. Sengupta, and S.M. Girvin, *Phys. Rev. B*

- 66**, 075128 (2002).
- 15 J. Simon, W.S. Bakr, R.C. Ma, M.E. Tai, P.M. Preiss, and M. Greiner, *Nature* **472**, 307 (2011).
  - 16 T. Matsubara and H. Matsuda, *Prog. Theor. Phys.* **16**, 416 (1956); *Prog. Theor. Phys.* **16**, 569 (1956); *Prog. Theor. Phys.* **17**, 19 (1957).
  - 17 R.A. Aziz, V.P.S. Nain, J.S. Carley, W.L. Taylor, and G.T. McConville, *J. Chem. Phys.* **70**, 4330 (1979).
  - 18 V.E. Korepin, N.M. Bogoliubov, and A.Z. Izergin, *Quantum inverse scattering method and correlation functions* (Cambridge, Cambridge University Press, 1993).
  - 19 M. Takahashi, *Thermodynamics of one-dimensional solvable models* (Cambridge, Cambridge University Press, 2005).
  - 20 A.O. Gogolin, A.A. Nersesyan, and A.M. Tsvelik, *Bosonization and strongly correlated systems* (Cambridge, Cambridge University Press, 1998).
  - 21 T. Giamarchi, *Quantum physics in one dimension* (Oxford, Oxford University Press, 2004).
  - 22 U. Schollwöck, *Rev. Mod. Phys.* **77**, 259 (2005).
  - 23 N. Kitanine, K.K. Kozłowski, J.M. Maillet, G. Niccoli, N.A. Slavnov, and V. Terras, *J. Stat. Mech.* P10009 (2007); *J. Stat. Mech.* P07010 (2008).
  - 24 R.G. Pereira, J. Sirker, J.-S. Caux, R. Hagemans, J.M. Maillet, S.R. White, and I. Affleck, *J. Stat. Mech.* P08022 (2007).
  - 25 H.E. Boos, J. Damerau, F. Göhmann, A. Klümper, J. Suzuki, and A. Weiße, *J. Stat. Mech.* P08010 (2008).
  - 26 F.H.L. Essler and R.M. Konik, *J. Stat. Mech.* P09018 (2009).
  - 27 N. Kitanine, K.K. Kozłowski, J.M. Maillet, N.A. Slavnov, and V. Terras, *J. Stat. Mech.* P04003 (2009); *J. Math. Phys.* **50**, 095209 (2009).
  - 28 N. Crampe, E. Ragoucy, and D. Simon, *J. Phys. A* **44**, 405003 (2011).
  - 29 A. Klauser, J. Mossel, J.-S. Caux, and J. van den Brink, *Phys. Rev. Lett.* **106**, 157205 (2011).
  - 30 K.K. Kozłowski and V. Terras, *J. Stat. Mech.* P09013 (2011).
  - 31 J. Sato, B. Aufgebauer, H. Boos, F. Göhmann, A. Klümper, M. Takahashi, and C. Trippe, *Phys. Rev. Lett.* **106**, 257201 (2011).
  - 32 A. Shashi, M. Panfil, J.-S. Caux, and A. Imambekov, *Phys. Rev. B* **85**, 155136 (2012).
  - 33 A. Luther and I. Peschel, *Phys. Rev. B* **12**, 3908 (1975).
  - 34 T. Hikihara and A. Furusaki, *Phys. Rev. B* **58**, R583 (1998); *Phys. Rev. B* **69**, 064427 (2004).
  - 35 S. Lukyanov and A. Zamolodchikov, *Nucl. Phys. B* **493**, 571 (1997).
  - 36 S. Lukyanov, *Phys. Rev. B* **59**, 11163 (1999).
  - 37 B. Pozsgay, *J. Stat. Mech.* P11017 (2011).
  - 38 S.D. Glazek and K.G. Wilson, *Phys. Rev. D* **48**, 5863 (1993); *Phys. Rev. D* **49**, 4214 (1994).
  - 39 F. Wegner, *Ann. Phys.* **3**, 77 (1994).
  - 40 A.H. MacDonald, S.M. Girvin, and D. Yoshioka, *Phys. Rev. B* **37**, 9753 (1988).
  - 41 M. Takahashi, *J. Phys. C: Solid State Phys.* **10**, 1289 (1977).
  - 42 A.L. Chernyshev, D. Galanakis, P. Phillips, A.V. Rozhkov, and A.-M.S. Tremblay, *Phys. Rev. B* **70**, 235111 (2004).
  - 43 J.-Y.P. Delannoy, M.J.P. Gingras, P.C.W. Holdsworth, and A.-M.S. Tremblay, *Phys. Rev. B* **72**, 115114 (2005).
  - 44 S. Müller, J. Billy, E.A.L. Henn, H. Kadau, A. Griesmaier, M. Jona-Lasinio, L. Santos, and T. Pfau, *Phys. Rev. A* **84**, 053601 (2011).
  - 45 A. Chotia, B. Neyenhuis, S.A. Moses, B. Yan, J.P. Covey, M. Foss-Feig, A.M. Rey, D.S. Jin, and J. Ye, *Phys. Rev. Lett.* **108**, 080405 (2012).
  - 46 C. Trefzger, C. Menotti, B. Capogrosso-Sansone, and M. Lewenstein, *J. Phys. B* **44**, 193001 (2011).
  - 47 M.P.A. Fisher, P.B. Weichman, G. Grinstein, and D.S. Fisher, *Phys. Rev. B* **40**, 546 (1989).
  - 48 M. Greiner, O. Mandel, T. Esslinger, T.W. Hansch, and I. Bloch, *Nature* **415**, 39 (2002).
  - 49 T. Stöferle, H. Moritz, C. Schori, M. Köhl, and T. Esslinger, *Phys. Rev. Lett.* **92**, 130403 (2004).
  - 50 I.B. Spielman, W.D. Phillips, and J.V. Porto, *Phys. Rev. Lett.* **98**, 080404 (2007).
  - 51 G.G. Batrouni, V. Rousseau, R.T. Scalettar, M. Rigol, A. Muramatsu, P.J.H. Denteneer, and M. Troyer, *Phys. Rev. Lett.* **89**, 117203 (2002).
  - 52 V.A. Kashurnikov, N.V. Prokofev, and B.V. Svistunov, *Phys. Rev. A* **66**, 031601 (2002).
  - 53 G. Campbell, J. Mun, M. Boyd, P. Medley, A.E. Leanhardt, L.G. Marcassa, D.E. Pritchard, and W. Ketterle, *Science* **313**, 5787 (2006).
  - 54 S. Fölling, A. Widera, T. Müller, F. Gerbier, and I. Bloch, *Phys. Rev. Lett.* **97**, 060403 (2006).
  - 55 F. Gerbier, A. Widera, S. Fölling, O. Mandel, T. Gericke, and I. Bloch, *Phys. Rev. Lett.* **95**, 050404 (2005).
  - 56 D. Clément, N. Fabbri, L. Fallani, C. Fort, and M. Inguscio, *Phys. Rev. Lett.* **102**, 155301 (2009).
  - 57 L. Fallani, J.E. Lye, V. Guarrera, C. Fort, and M. Inguscio, *Phys. Rev. Lett.* **98**, 130404 (2007).
  - 58 T.D. Kühner, S.R. White, and H. Monien, *Phys. Rev. B* **61**, 12474 (2000).
  - 59 L. Amico and V. Penna, *Phys. Rev. B* **62**, 1224 (2000).
  - 60 V.W. Scarola and S. Das Sarma, *Phys. Rev. Lett.* **95**, 033003 (2005).
  - 61 D.L. Kovrizhin, G.V. Pai, and S. Sinha, *Europhys. Lett.* **72**, 162 (2005).
  - 62 G.G. Batrouni, F. Hebert, and R.T. Scalettar, *Phys. Rev. Lett.* **97**, 087209 (2006).
  - 63 T. Mishra, R.V. Pai, S. Ramanan, M.S. Luthra, and B.P. Das, *Phys. Rev. A* **80**, 043614 (2009).
  - 64 M.A. Cazalilla, R. Citro, T. Giamarchi, E. Orignac, and M. Rigol, *Rev. Mod. Phys.* **83**, 1405 (2011).
  - 65 R. Fazio and H. van der Zant, *Phys. Rep.* **355**, 235 (2001).
  - 66 G. Grignani, A. Mattoni, P. Sodano, and A. Trombettoni, *Phys. Rev. B* **61**, 11676 (2000).
  - 67 L.I. Glazman and A.I. Larkin, *Phys. Rev. Lett.* **79**, 3736 (1997).
  - 68 D. Giuliano and P. Sodano, *Nucl. Phys. B* **711**, 480 (2005).
  - 69 D. Giuliano and P. Sodano, *New Journal of Physics* **10**, 093023 (2008); *Nucl. Phys. B* **811**, 395 (2009).
  - 70 D. Giuliano and P. Sodano, *Europhys. Lett.* **88**, 17012 (2009); *Nucl. Phys. B* **837**, 153 (2010).
  - 71 A. Cirillo, M. Mancini, D. Giuliano, and P. Sodano, *Nucl. Phys. B* **852**, 235 (2011).
  - 72 E. Altman and A. Auerbach, *Phys. Rev. Lett.* **89**, 250404 (2002).
  - 73 F.D.M. Haldane, *Phys. Rev. Lett.* **50**, 1153 (1983).
  - 74 H.J. Schulz, *Phys. Rev. B* **34**, 6372 (1986).
  - 75 E.G. Dalla Torre, E. Berg, and E. Altman, *Phys. Rev. Lett.* **97**, 260401 (2006); E. Berg, E.G. Dalla Torre, T. Giamarchi, and E. Altman, *Phys. Rev. B* **77**, 245119 (2008).
  - 76 L. Amico, G. Mazzarella, S. Pasini, and F.S. Cataliotti, *New J. Phys.* **12**, 013002 (2010).



- <sup>77</sup> M. Dalmonte, M. Di Dio, L. Barbiero, and F. Ortolani, Phys. Rev. B **83**, 155110 (2011).
- <sup>78</sup> D. Rossini and R. Fazio, New J. Phys. **14**, 065012 (2012).
- <sup>79</sup> S. Eggert and I. Affleck, Phys. Rev. B **46**, 10866 (1992).
- <sup>80</sup> S. Lukyanov and V. Terras, Nucl. Phys. B **654**, 323 (2003).
- <sup>81</sup> Since only eigenstates with zero total spin along the  $z$  axis are physically meaningful (due to the constraint on the total number of particles), in the following we use the formulas of Ref. 34 at vanishing applied magnetic field.
- <sup>82</sup> F. Mila and K.P. Schmidt, *Strong-Coupling Expansion and Effective Hamiltonians*, Chap. 19 of Ref. 2.
- <sup>83</sup> J.K. Freericks and H. Monien, Phys. Rev. B **53**, 2691 (1996).
- <sup>84</sup> Since  $[S, \mathcal{P}] \neq 0$ ,  $H_I$  is different from  $\tilde{H}_I = S^\dagger H_I S$ .
- <sup>85</sup> Although the contribution to the total energy arising from magnetic fields vanishes on the physical states due to the constraint on the particle number, in the intermediate calculations one has to retain it when computing the redefined XXZ parameters.
- <sup>86</sup> Notice that, as discussed in the following, the constraint on the total number (implying that only states of the XXZ model with the  $z$  component of the total spin equal to zero may be realized within the BH model in the canonical ensemble) does not affect the spin liquid / Néel-Ising phase transition since it just implies the existence of (at least two) ferromagnetic domain walls, in the ferromagnetic-Ising phase of the XXZ model.
- <sup>87</sup> S. Kehrein, *The flow equation approach to many-particle systems* (Berlin, Springer Verlag, 2006).
- <sup>88</sup> This result does not depend on the particular choice of  $r_{\max}$ .
- <sup>89</sup> In passing we point out that, to obtain more accurate results on the phase transition points, a finite-size scaling of the data with  $L$  is needed. Namely, one should estimate the value of  $\Delta_{\text{eff}}^{AF/F}$  for different sizes  $L$ , and then perform a fit of that quantity with  $L$ , such to extrapolate the thermodynamic limit. This analysis lies beyond our present purposes, which are to provide estimates of the transition within a precision of  $\approx 5\%$ .
- <sup>90</sup> T. Prosen, Phys. Rev. Lett. **106**, 217206 (2011); Phys. Rev. Lett. **107**, 137201 (2011).
- <sup>91</sup> M. Campostrini and E. Vicari, Phys. Rev. Lett. **102**, 240601 (2009); Phys. Rev. A **81**, 063614 (2010).
- <sup>92</sup> J. Carrasquilla, F. Becca, A. Trombettoni, and M. Fabrizio, Phys. Rev. B **81**, 195129 (2010).
- <sup>93</sup> I. Affleck, J. Phys. A **31**, 2761 (1998).
- <sup>94</sup> Notice that computing the renormalization of the effective XXZ parameters via the Luttinger treatment done in Sec. IV with periodic boundary conditions is enough to give excellent agreement with BH numerical data, provided that, of course, the correlation functions of the XXZ model are computed for open boundary conditions according to Eqs. (14, 15).